UNIVERSITA' DEGLI STUDI DI PADOVA
FACOLTA' DI INGEGNERIA
DIPARTIMENTO DI INGEGNERIA IDRAULICA, MARITTIMA,
AMBIENTALE E GEOTECNICA

TESI DI DOTTORATO

NUMERICAL MODELLING OF ALLUVIAL RIVERS BY SHOCK CAPTURING METHODS

SUPERVISORI: Ch.mo Prof. Luigi D'Alpaos, Ch.mo Prof. Stefano Lanzoni,
Ch.mo Prof. Andrea Defina
CORRELATORE: Ing. Nunzio Siviglia
CONTRORELATORE: Ch.mo Prof. Sergio Fagherazzi

DOTTORANDO: ALBERTO CANESTRELLI

ANNO ACCADEMICO 2007-2008

Ai miei genitori

Contents

List of Figures

List of Tables

Abstract

The problem of modelling both the unsteady hydrodynamics and the bed morphological variations in natural channels is generally performed by solving the De Saint Venant balance equations for the liquid phase together with the Exner continuity equation for the sediments carried as bed-load. This thesis focuses on the development of an high-order accurate centred scheme of the finite volume type for the numerical solution of the coupled De Saint Venant-Exner system. A new scheme, called PRICE-C, is proposed. It solves the system of equations in a non-conservative form, however it has the important characteristic of reducing automatically to a conservative scheme if the underlying PDE system is a conservation law. It is applied to the shallow water equations in the presence of either a fix or a movable bed. The scheme is first introduced in a one-dimensional framework, and it is then extended to the two-dimensional case. The extension is not straightforward in the case of an unstructured mesh, since averages over suitable edge-based control volumes have to be performed.

The scheme is extended to high order of accuracy in space and time via the ADER-WENO and MUSCL technique respectively for the one- and two-dimensional case. The well-balanced property of the scheme is proven, i.e. the ability to reach steady states also in the presence of discontinuous water surface or discontinuous bottom profile. The scheme can deal with subcritical and supercritical flows, as well as transcritical situations. Moreover the proposed approach leads to a correct estimate of the celerity of surface discontinuities as

well sediment bores and small bottom perturbations.

The main characteristic of the scheme is its simplicity: it is based on a simple centred approach, that means that the knowledge of the eigenvalues of the matrix of the system is not required. This is important since the interaction between sediment transport and water flow not always admits detailed knowledge of the eigenstructure. Hence this scheme can be useful to engineers since they need simple numerical tools that can be easily used without entering in the mathematical detail of the differential hyperbolic system under consideration. Moreover the centred strategy gives generality to the scheme: in fact, it can be applied without modification to any kind of hyperbolic equations with non-conservative terms.

Sommario

La modellazione dell'idrodinamica e delle variazioni morfologiche in canali naturali è generalmente effettuata risolvendo numericamente le equazioni delle onde lunghe in acque basse, che regolano il moto della fase fluida, assieme all'equazione di Exner, che descrive l'evoluzione del fondo. L'argomento della presente tesi consiste nello sviluppo di un schema ai volumi finiti di tipo "centrato" per la soluzione accoppiata di tale sistema di equazioni. Un nuovo schema, denominato PRICE-C, è qui introdotto: esso risolve le equazioni in forma non-conservativa, ma ha l'importante proprietà di degenerare in uno schema conservativo se il sottostante sistema di equazioni ammette una forma conservativa. Lo schema è applicato alle equazioni delle onde lunghe in acque basse sia nel caso di fondo fisso che di fondo mobile, dapprima in un ambito unidimensionale e successivamente in quello bidimensionale. L'estensione non è immediata nel caso in cui il reticolo di calcolo sia non-strutturato, dal momento che le equazioni differenziali devono essere mediate su opportuni volumi di controllo.

Lo schema è poi esteso ad alti ordini di accuratezza nello spazio e nel tempo attraverso le procedure ADER-WENO e MUSCL rispettivamente per il caso unidimensionale e bidimensionale.

Inoltre si dimostra come lo schema proposto verifichi la "well-balanced property", che consiste nella capacità di raggiungere soluzioni stazionarie, anche in presenza di discontinuità della superficie libera e del fondo. Condizioni di corrente lenta e rapida, come pure condizioni di tipo transcritico vengono correttamente

risolte. Inoltre lo schema in grado di riprodurre le celerità di propagazione di discontinuità della superficie e fronti di sedimenti al fondo, così come la celerità di propagazione di piccoli disturbi del fondo.

Caratteristica principale dello schema è la sua semplicità: è basato su un semplice approccio di tipo centrato, cioè non necessita la conoscenza degli autovalori della matrice del sistema. Questa è un'importante caratteristica dal momento che non sempre autovalori e autovettori sono calcolabili analiticamente, in particolare nel caso di complesse formule di chiusura per il trasporto al fondo. Quindi questo schema può rivelarsi utile per l'ingegnere che spesso necessita di un semplice strumento numerico che possa essere applicato ad un sistema di equazioni differenziali di tipo iperbolico senza dover entrare nel dettaglio delle proprietà matematiche del sistema stesso. Data la sua generalità, infatti, lo schema può essere applicato ad ogni tipo di sistema iperbolico contenente termini non-conservativi.

Chapter 1

Introduction

Sediment transport is a fundamental aspect of fluvial hydraulics. Indeed, river beds always tend to an asymptotic equilibrium strongly affected by the two transported phases: water and sediments. The river morphology may be altered by natural (floods) or man-induced (river training works) perturbations. These perturbations may lead to significant morphological changes in the bed profile. Quantifying the interaction between sediment transport and water flow is crucial for a wide range of phenomena such as river morphodynamic evolution, river management, and river adjustment after the installation of hydraulic structures. To progress on quantifying such interactions, it becomes necessary to develop numerical models that accurately simulate the fluid flow over a movable bed. This thesis focuses on the numerical modelling of river hydrodynamics and morphodynamics with particular attention to physical phenomena in which water surface discontinuities and sediment bores are present.

A typical example of an unsteady water surface discontinuity is the shock wave forming after a sudden dam removal (dam-break problem), that causes a rarefaction wave to propagate upstream, whereas a shock propagates downstream. The dam-break problem is usually used as test case for numerical models, since an exact solution exists for the frictionless case with horizontal bed.

Another discontinuous wave phenomenon that can be found in river estuaries is the tidal bore. A tidal bore is a tidal phenomenon in which the landward edge of the incoming tide forms a steep wave of water that travel up a river against the direction of the current. Bores occur usually in areas with a large tidal range (typically more than 3-4 m between high and low water), and where incoming tides are funnelled into a shallow, narrowing river via a broad bay. These are examples of unsteady waves, whereas a stationary discontinuous wave that is frequently observed in open channel flow such as rivers and spillways is the so called "hydraulic jump". When flow at high enough velocity discharges into a zone of lower velocity, a rather abrupt rise (a step or standing wave) occurs in the water surface. The supercritical flowing water is abruptly slowed and increases in height converting some of the flow's initial kinetic energy into an increase in potential energy, with some energy irreversibly lost through turbulence to heat. In the case of a movable bed, also if the hydrodynamic boundary conditions are steady, the hydraulic jump can slowly move and a corresponding sediment bore can form at the bottom (Bellal et al., 2003).

The common tool to predict river hydrodynamics and morphodynamics are the shallow water equations (or De Saint Venant equations) and the Exner sediment balance equations (see e.g. Cunge et al., 1980; Graf and Altinakar, 1998), where friction head loss and solid transport are estimated by closure equations. In the last two decades a lot of numerical models solving these equations were developed. Two different approaches are present in literature. The first is the uncoupled approach, where the hydrodynamic equations are solved separately from the Exner equation: the computed hydrodynamic unknowns are then passed to the morphodynamic module (and vice versa) at the end of each time steps (see, among others, Cunge and Perdreau, 1973; Krishnappan, 1985; Defina, 2003; Wu et al., 2004). The uncoupled strategy was justified because of the different time scales of flow and sediment transport and the inherent inaccuracies introduced by the use of empirical formulas for bed roughness and sediment transport capacity. The second approach relies on a full coupling of the governing equations within each time step (see, among others, Lyn, 1987; Holly and Rahuel, 1990; Lai, 1991;

Correia et al., 1992; Saiedi, 1997; Kassem and Chaudry, 1998; Cao et al., 2002; Crnjaric-Zic et al., 2003; Cao et al., 2004; Hudson and Sweby, 2005; Caleffi et al., 2007). Saiedi (1997) and Cao et al. (2002) compared the numerical stability of coupled and decoupled models, founding out that the coupled model is more stable, especially in the case of rapid variation of bottom elevation. Moreover, Cao et al. (2002) and Correia et al. (1992) pointed out that coupled solutions should be used for the study of long term evolutions of natural rivers. Sieben (1997; 1999) showed that in a range near to critical conditions, the coupling between the shallow water equations and the Exner equation within the time step is crucial. Close to critical condition in fact, each of the wave propagation celerities can no longer be identified solely with a surface wave or solely with a bed wave, and a full coupling of the equations is necessary to correctly solve the propagation of bed disturbances. The range of Froude number for which coupling is fundamental is not fixed, but it depends on the sediment concentration: the larger is the sediment transport, the larger is the range within which the uncoupled model gives incorrect results. Moreover, as discussed by Lanzoni et al. (2006), simulating the evolution of fairly short perturbation near critical conditions by means of a decoupled approach does not account for morphodynamic influence (i.e. propagation of information on bed variations) either upstream or downstream, whereas only a coupled approach is able to propagate bed information in both directions. On the contrary, very long bottom waves, even if transcritical, display a quasi-diffusional behaviour which can be satisfactorily modelled using a decoupled approach.

An other important issue suggesting for the adoption of a coupled strategy in morphodynamic models is related to the boundary conditions. Lyn (1987) investigated the coupling between flow and sediment dynamics in situations where both the fluid and the sediment discharge are rapidly changing, showing that decoupled models are not capable of satisfying either a general boundary condition or an arbitrary initial condition.

Therefore, adopting a coupled approach for solving the governing equations is a stringent requirement in order to obtain reliable results when flow is close to

critical conditions and the boundary conditions are rapidly changing, a situation that characterizes most mountain rivers and, at least locally, is often encountered in natural rivers due to the presence of bridge piers, flood control systems and sudden variations in bed slope or river width.

Several numerical methods are available to solve the set of equations governing morphodynamic. As far as finite difference scheme are concerned, a very popular method is the implicit Preissmann finite difference scheme (Preissmann, 1961; Cunge and Perdreau, 1973), used for example by Holly and Rahuel (1990) and Correia et al. (1992). This implicit scheme allows large time steps, but has the short coming that, in the case of fixed bed, is not able to model transcritical flows (Meselhe and Holly, 1997). Indeed, it does not allow imposing conflicting boundary conditions (e.g. the water depth both at the upstream and downstream end of the computational domain at the same time). Another class of schemes, of the finite-volume type, had a great increase of popularity in the last decades. The finite-volume Schemes on the one hand use a smaller time step because they have to satisfy the Courant-Friedrichs-Levy (CFL) condition. On the other hand they have the advantage of the flexibility in imposing the boundary conditions and they are usually "shock-capturing".

In most of the aforementioned studies, the coupled system is solved without particular attention to the mathematical form of the system of equations to be solved numerically, in particular in the presence of shock waves. Often, a non-conservative formulation of the system is considered (Correia et al., 1992; Saiedi, 1997; Lai, 1991), that however gives good results as far as the solution is smooth. In the presence of discontinuities, it is well known that a non-conservative (primitive) formulation of the numerical solution leads to a wrong computation of the height and speed of the jumps, thus rendering rapidly meaningless long term morphodynamic simulations in the presence of shocks or sediment bores. Even when equations are recast in conservative form, non-conservative terms are usually treated as source terms (Cao et al., 2002; Crnjaric-Zic et al., 2003; Cao et al., 2004; Hudson and Sweby, 2005; Caleffi et al., 2007). In the present thesis we instead take advantage of the definition of weak solutions in presence of

non-conservative products (Dal Maso et al., 1995). Clearly, the implementation of a model that is able to deal with discontinuous solutions and different kind of transport closure equations turns out to be more complicated in a coupled framework. The celerities of propagation of both small and finite perturbations (i.e., the eigenstructure of the system) are in fact different from the fixed bed case and change with the adopted transport formula. This is one of the reasons for which the decoupled models are still so popular.

The aim of this thesis it is to develop an original numerical tool that can be applied to any kind of hyperbolic equations with non-conservative term. In particular, the new scheme is applied to the De Saint Venant-Exner equations, in order to deal with subcritical and supercritical flows, as well as transcritical situations. Moreover the proposed approach leads to a correct estimate of the celerity of surface discontinuities as well sediment bores and small bottom perturbations.

In this work only bed-load transport is considered. The reason is to be found in the fact that once the suspended load equation is added to the coupled De Saint Venant-Exner system, it does not change the eigenstructure of the system itself, i.e. the speed of propagation of the perturbations. In fact, the matrix of the system has a new eigenvalue ($\lambda = u$) and the other eigenvalues do not change (Toro, 2001). Non-equilibrium transport is also neglected in the present work. This assumption, implying instantaneous adaptation of the transport to the current, is usually satisfied for bed-load conditions, whereas non-equilibrium effects may play some role for dominant suspended-load.

The thesis is organized as follows. In chapter 2 a literature review of finite volume schemes is provided. The original finite volume scheme is introduced within a one-dimensional framework. In chapter 3 the performance of the proposed high order algorithm is checked for the system of time-dependent non-linear shallow water equations without and with sediment transport. The scheme is tested against both analytical solutions and real situations for which experimental data are available. In particular the numerical model is compared with the experimental case of an hydraulic jump forming over a movable bed (Bellal et al.,

2003). This transcritical flow, resulting from conflicting boundary conditions (water level imposed upstream and downstream), is challenging for numerical modelling. Indeed, a sudden change in the downstream boundary conditions forces a flow discontinuity in the channel, which can be managed if boundary conditions are well posed and if the internal solver is shock-capturing. Chapter 4 describes the extension of the numerical scheme to a multi-dimensional framework. The extension is not straightforward in the case of an unstructured mesh, since an average over suitable edge-based control volumes has to be performed. In chapter 5 the two-dimensional version of the scheme is applied to the shallow water equations with either a fixed and a movable bed, and a comparison with analytical solutions and with solutions that are present in literature is performed. Conclusions and possible further developments are drawn in chapter 6.

Chapter 2

One-dimensional PRICE-C scheme

In the recent years, high resolution methods for hyperbolic systems of conservation laws have been developed and extensively applied for solving shallow water equations, frequently used in fluid mechanics and hydraulic engineering. Much effort was devoted to design high-accuracy schemes to reduce the number of computational cells and minimize the computational time. In particular, the finite volume method (FVM) had undergone a great increase of popularity in the last decades. One advantage of the finite volume method over the finite difference method is that it does not require a structured mesh (although a structured mesh can be used), and hence it can deal easily with irregular geometries. Furthermore, the finite volume method, unlikely the finite element method, can easily conserve the variables on a coarse mesh, an important requirement especially for fluid dynamic problems. Moreover, since it usually makes use of the conservative form of the governing equations, the FVM allows to deal easily with discontinuities of the solution. In the following, a review of finite volume schemes of the centred and upwind type is presented. The new PRICE-C scheme of the centred type is then introduced in a one-dimensional framework.

2.1 Literature review of finite volume schemes

In the last three decades, there has been a tremendous progress in the development and improvement of finite volume methods of both upwind and central type. Upwind methods have their origin in the work of Courant, Isaacson, and Rees (1952), and most of all, in the work of Godunov (1959). But the real advance of these methods came in the late 70's and 80's, starting with the works of van Leer, Osher, Roe, Harten and many others (for a general overview, the reader is referred to Toro, 1999; 2001; LeVeque, 2002). Upwind schemes are physically based, have a characteristic-wise structure that allows to obtain a better resolution of shocks, but require extensive and expensive use of the eigenstructure. Usually the global solution is achieved via local solutions of Riemann problems, approximate or exact. The Riemann problem consists in solving the system of partial differential equations (PDE) starting from an initial condition characterized by constant states in each single cell (Fig. 2.1). For most known hyperbolic systems, the exact or approximate solution of the Riemann problem is available, although in some cases this may be computationally very expensive. However there are complicated hyperbolic systems where the solution of the Riemann problem is not available.

The alternative approach is the centred scheme family, whose origins are the first-order Lax-Friedrichs staggered method (Lax, 1954) and the second-order Nessyahu-Tadmor staggered method (Nessyahu and Tadmor, 1990). In a centred framework, the initial condition is again a Riemann problem, but the update is obtained integrating the PDE equations in particular space-time control volumes, so that the Riemann problem is not explicitly computed. The centred schemes are very simple due to their component-wise structure, and very flexible owing to the minimum use of eigenvalues. They just need a superior limit of the spectral radius for stability requirements, that can be always calculated numerically also for complicated systems of equations. Third-order extension of Nessyahu-Tadmor type schemes can be found in Liu and Tadmor (1998) and Jiang et al. (1998), respectively in a staggered and non-staggered version. This method was

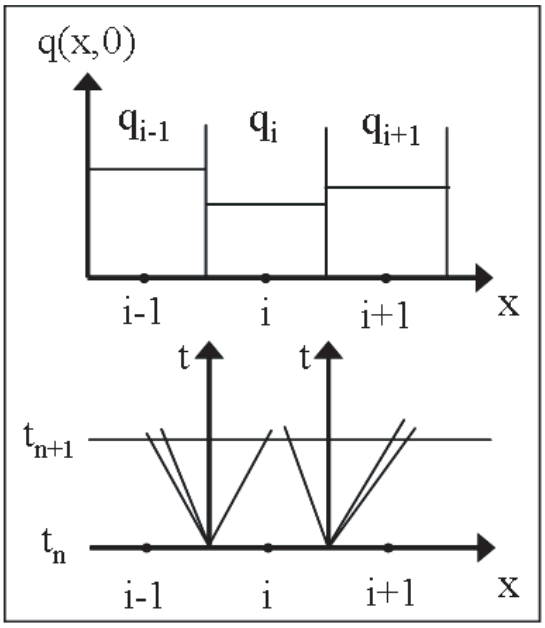

Figure 2.1: In the upper part: the initial condition characterized by constant states. In the lower part: the propagation waves starting at each interface are shown. The global solution at time t_{n+1} is achieved via local solutions of Riemann problems.

also extended to two-dimensional cartesian (Jiang and Tadmor, 1998) and unstructured (Arminjon et al., 1997; Arminjon and Viallon, 1999; Kuther, 2001) grids and to three dimensional problems (Arminjon and St-Cyr, 2003). Three dimensional cartesian, adaptive grids were discussed by Noelle et al. (2006).

In Bianco et al. (1999) and Levy et al. (1999) a new family of high-order schemes for one-dimensional problems was introduced. This family was based on the reconstruction of the point-values of conservative variables and flux derivatives by ENO and WENO (Shu, 1997) methods and on the combination of the natural continuous extension procedure (Zennaro, 1986) with a Runge-Kutta solver in time. The independence from the eigensystem of the scheme and the consequent component-wise structure were described as the main advantages of these new methods. Extension to two-dimensional cartesian grids was provided

by Levy et al. (2002). Qiu and Shu (2002) performed a comparison between central staggered WENO high-order methods with RungeKutta solver in time, either using or not using the local characteristic decomposition. Such a decomposition was shown to improve the results when the structure of the shocks is quite complex and the order of accuracy of the method is very high. In the work of Pareschi et al. (2005) on the central Runge-Kutta schemes the quadrature rule in time for the fluxes is avoided, so further improving the efficiency.

Kurganov and Tadmor (2000), using a variable control volume, introduced new central semi-discrete and fully discrete non-staggered schemes, based on the use of local propagation celerities. Kurganov and Petrova (2005) extended this schemes to unstructured grids in two-dimensional problems. Liu (2005) introduced overlapping cell representation of the solution. Although the use of overlapping cells generally doubles the computational cost, more efficient reconstruction methods using the combined information from the overlapping cell averages could improve the resolution (see also Liu et al., 2007; Li, 2008, for recent developments). In all the above Kurganov-type schemes the use of the semi-discrete form allows to avoid grid staggering, introducing significant simplifications when multi-dimensional problems are tackled. Nevertheless, these schemes use a certain amount of upwind information through the estimation of maximum wave speed at each computational cell.

A given numerical scheme, when applied to conservation laws with source terms, (i.e. the shallow water equations) all numerical schemes should satisfy the well-balanced property (or C-property). This property guarantees the balance between the flux gradient and the bed-slope term when the flow is stationary. The first important result in computing such solutions was given by Bermudez and Vazquez (1994) that introduced the first order Q-scheme and the idea of source term upwinding. An improvement of this scheme can be found in Vazquez-Cendon (1999). Garcia-Navarro and Vazquez-Cendon (2000) analyzed the source term due to cross section irregularities and Hubbard and Garcia-Navarro (2000) analyzed the effects of source terms in a flux difference splitting technique. LeVeque (1998) developed a wave propagation algorithm by solving

the Riemann problem at the cell center and cancelling the source term exactly with the flux difference. Zhou et al. (2001; 2002) introduced, for the shallow water equations, the surface gradient method (SGM), that uses the water surface level, instead of conservative variables, to reconstruct the Riemann states at the cell interfaces. Bryson and Levy (2005) extended the Kurganov type schemes to guarantee their application and the well-balanced property in the shallow water equations with bed slope source term (see also Kurganov and Petrova (2007)). In Vukovic and Sopta (2002), the C-property was exactly satisfied, but the method is quite complex. Xing and Shu (2006) generalized Runge-Kutta finite volume WENO schemes and Runge-Kutta discontinuous Galerkin (RKDG) finite element methods to obtain high order well-balanced schemes. High accuracy and well-balancing are also obtained by Crnjaric-Zic et al. (2004) using both finite volume WENO and central WENO schemes. Levy et al. (1999) WENO scheme was recently generalized to gain the well-balanced property by Caleffi et al. (2006; 2007).

The use of these method listed above, designed to solve the conservative form of the equations, is fundamental when the computational domain is characterized by internal discontinuities. Indeed, when solutions are smooth there is no good reason why one should not use a non-conservative (or "primitive") method. In practice these methods perform very well (Toro, 1998) and in fact there are situations in which non-conservative methods outperform conservative methods (Toro, 2002). However, shock waves are computed with the wrong strength and the wrong propagation speed, in according withHou and LeFloch (1994) theorem proving that non-conservative methods will converge to the wrong solution in the presence of a shock wave. As a consequence, when a discontinuous solution is sought, the equations should be recast in conservative form. In all the above mentioned works, non-conservative terms (i.e. terms that can not be recast in conservative form) were usually treated as source terms, and different procedures were proposed to balance them with the fluxes in order to satisfy the C-property. Only in the last few years, attempts have been done to solve the equations written in a way that non-conservative terms are recast together with the fluxes

in a non-conservative form (Parés and Castro, 2004; Castro et al., 2006; Gallardo et al., 2007; Castro et al., 2008a;b). These schemes make use of the theory of Dal Maso et al. (1995), that provides a definition of weak solutions in presence of non-conservative products. Parés and Castro (2004), in particular, introduced a well-balanced high order scheme of the upwind type, using the generalization of the Roe method to non-conservative systems, that allows to preserve the shock capturing property of the scheme. The scheme was applied to the shallow water equations with fixed bed. The extension to the movable-bed case was recently proposed by Castro et al. (2008b).

The new scheme introduced in this thesis use the theory of Dal Maso et al. (1995) to solve the equations in non-conservative form and it is proven to degenerate to the FORCE conservative scheme (Toro, 1996) when non-conservative terms are neglected. The main characteristic of the scheme is its simplicity: it is based on a simple centred approach, because the interaction between sediment transport and water flow not always admits detailed knowledge of the eigenstructure. Moreover the well-balanced property of the scheme is proven for the shallow water equations, with both mobile and fix bed and over continuous and discontinuous bottom profiles. This is extremely important in the movable-bed case, because the well-balancing of the scheme allows to reproduce small perturbations of the free surface and of the bottom elevation, otherwise of the same order of magnitude of the numerical errors induced by the non-balancing. This work represents the first attempt to solve a non-conservative system using the theory of Dal Maso et al. (1995) by a centred approach. The strength of the present method consists of a large applicability in a broad range of engineering problems, since no mention is done to the eigenstructure of the hyperbolic system of equations. In this chapter only one-dimensional flow is considered, whereas the two-dimensional version of the scheme is described in chapter 4.

2.2 Description of the numerical scheme

Let us consider a system of partial differential equations of the form:

$$\frac{\partial \mathbf{Q}}{\partial t} + \mathbf{A}\frac{\partial \mathbf{Q}}{\partial x} = 0 \qquad , \qquad x \in \mathbb{R}, t > 0 \tag{2.1}$$

in which $\mathbf{Q} = [q_1, \dots q_N]^T$ is the vector of unknowns and $\mathbf{A} = \mathbf{A}(\mathbf{Q})$ is the coefficient matrix (hereinafter all vectors and matrices will be denoted by bold characters). It is assumed that the unknown function $\mathbf{Q}(x,t)$ takes its values inside an open convex set Ω included in $\mathbb{R}$ and that $\mathbf{Q} \in \Omega \rightarrow \mathbf{A}(\mathbf{Q})$ is a smooth locally bounded map. System (2.1) is assumed to be hyperbolic with real eigenvalues $\lambda_1, \lambda_2, \dots \lambda_N$ and a set of corresponding linearly independent right eigenvectors $R(1), \dots, R(n)$. The numerical method developed here is of the centred type and it only requires an estimate for the absolute value of the maximum eigenvalue in order to satisfy the stability condition. Hereinafter the vector of unknowns $\mathbf{Q}$ in (2.1) will be the vector of physically conserved variables. Therefore, if $\mathbf{A}(\mathbf{Q})$ is the Jacobian matrix $\mathbf{A}(\mathbf{Q}) = \partial\mathbf{F}/\partial\mathbf{Q}$, with $\mathbf{F} = \mathbf{F}(\mathbf{Q})$, the physical flux (2.1) can be expressed in the conservative form:

$$\frac{\partial \mathbf{Q}}{\partial t} + \frac{\partial \mathbf{F}}{\partial x} = 0 \tag{2.2}$$

Toro and Siviglia (2003) developed a series of primitive centred (PRICE) numerical schemes for solving systems of hyperbolic partial differential equations written in the non-conservative form (2.1). The most promising of these schemes, namely the PRICE-T scheme, will be the basis of the high-order centred scheme developed in the present thesis.

2.2.1 The FORCE scheme and the original two-steps PRICE-T scheme

Since the PRICE-T scheme Toro and Siviglia (2003) is the non-conservative analogous of the conservative FORCE scheme Toro (1996), that is in turn a deterministic re-interpretation of the staggered-grid version of the Random Choice Method (RCM) of Glimm (1965), the definition of the FORCE scheme for conservation laws is briefly recalled here. The FORCE scheme for the conservative system (2.2) can be written either in a two-step staggered grid version as

- first step: computation of the intermediate state

$$\mathbf{Q}_{i+\frac{1}{2}}^{n+\frac{1}{2}} = \frac{1}{2}(\mathbf{Q}_i^n + \mathbf{Q}_{i+1}^n) - \frac{1}{2}\frac{\Delta t}{\Delta x}\left[\mathbf{F}(\mathbf{Q}_{i+1}^n) - \mathbf{F}(\mathbf{Q}_i^n)\right], \tag{2.3}$$

- second step: update formula

$$\mathbf{Q}_i^{n+1} = \frac{1}{2}\left(\mathbf{Q}_{i-\frac{1}{2}}^{n+\frac{1}{2}} + \mathbf{Q}_{i+\frac{1}{2}}^{n+\frac{1}{2}}\right) - \frac{1}{2}\frac{\Delta t}{\Delta x}\left(\mathbf{F}(\mathbf{Q}_{i+\frac{1}{2}}^{n+\frac{1}{2}}) - \mathbf{F}(\mathbf{Q}_{i-\frac{1}{2}}^{n+\frac{1}{2}})\right), \tag{2.4}$$

or in the more convenient conservative non-staggered one-step formulation with two-point fluxes as

$$\mathbf{Q}_i^{n+1} = \mathbf{Q}_i^n - \frac{\Delta t}{\Delta x}\left[\mathbf{F}_{i+\frac{1}{2}}^{FORCE} - \mathbf{F}_{i-\frac{1}{2}}^{FORCE}\right]. \tag{2.5}$$

Here, the FORCE flux $\mathbf{F}_{i+\frac{1}{2}}^{FORCE}$ is the arithmetic average of the Lax-Friedrichs and the Lax-Wendroff fluxes, i.e.

$$\mathbf{F}_{i+\frac{1}{2}}^{FORCE} = \frac{1}{2}\left(\mathbf{F}_{i+\frac{1}{2}}^{LF} + \mathbf{F}_{i+\frac{1}{2}}^{LW}\right), \tag{2.6}$$

with the Lax-Friedrichs flux

$$\mathbf{F}_{i+\frac{1}{2}}^{LF} = \frac{1}{2}\left(\mathbf{F}(\mathbf{Q}_{i+1}^n) + \mathbf{F}(\mathbf{Q}_i^n)\right) - \frac{1}{2}\frac{\Delta x}{\Delta t}\left(\mathbf{Q}_{i+1}^n - \mathbf{Q}_i^n\right), \tag{2.7}$$

and the Lax-Wendroff flux

$$\mathbf{F}_{i+\frac{1}{2}}^{LW} = \mathbf{F}\left(\mathbf{Q}_{i+\frac{1}{2}}^{n+\frac{1}{2}}\right), \tag{2.8}$$

where $\mathbf{Q}_{i+\frac{1}{2}}^{n+\frac{1}{2}}$ is given by (2.3). It is easy to prove via simple algebraic manipulations that the two schemes (2.3) & (2.4) and (2.5) are identical. However, for the purpose of this thesis the Lax-Wendroff flux as given in (2.3) & (2.8), is not convenient. The main problem consists of its two-step nature, leading to a non-linear numerical flux function with respect to the arguments $\mathbf{Q}_i^n$, $\mathbf{Q}_{i+1}^n$, $\mathbf{F}(\mathbf{Q}_i^n)$ and $\mathbf{F}(\mathbf{Q}_{i+1}^n)$, which makes it cumbersome for further analytic manipulations, since any further assumptions on $\mathbf{F}$, other than hyperbolicity, is not desirable. In this thesis the following variant of the conservative FORCE flux is therefore proposed:

$$\mathbf{F}_{i+\frac{1}{2}}^{FORCE'} = \frac{1}{2}\left(\mathbf{F}_{i+\frac{1}{2}}^{LF} + \mathbf{F}_{i+\frac{1}{2}}^{LW'}\right), \tag{2.9}$$

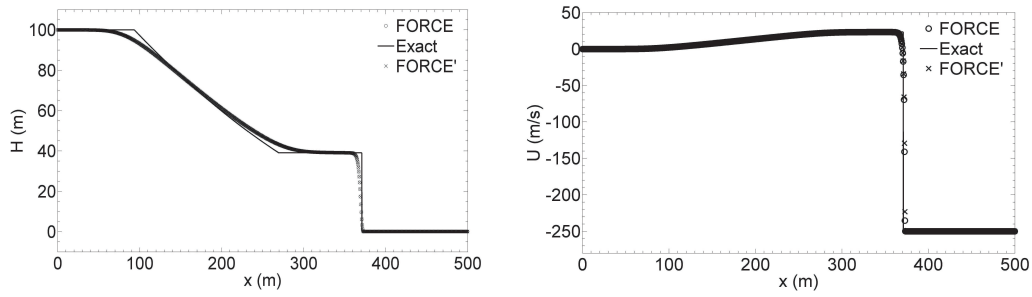

Figure 2.2: Comparison between the FORCE scheme and the modified FORCE scheme (FORCE') applied to the inviscid dam break problem generating a strong shock wave (initial conditions $h_l = 100m$, $h_r = 0.1m$, $u_l = 0$ and $u_r = -250m/s$, the subfixes "l" and "r" denoting left and right conditions, respectively). Results correspond to t =5 s and 1000 cells have been used in the simulations. The longitudinal distributions of the water profile with the two schemes are almost indistinguishable. The continuous line denotes the exact analytical solution.

where the modified Lax-Wendroff-type flux is now given by

$$\mathbf{F}^{LW'}_{i+\frac{1}{2}} = \frac{1}{2}\left(\mathbf{F}(\mathbf{Q}^n_{i+1}) + \mathbf{F}(\mathbf{Q}^n_i)\right) - \frac{1}{2}\frac{\Delta t}{\Delta x}\widehat{\mathbf{A}}_{i+\frac{1}{2}}\left(\mathbf{F}(\mathbf{Q}^n_{i+1}) - \mathbf{F}(\mathbf{Q}^n_i)\right). \qquad (2.10)$$

The matrix $\widehat{\mathbf{A}}_{i+\frac{1}{2}} = \widehat{\mathbf{A}}_{i+\frac{1}{2}}(\mathbf{Q}^n_i, \mathbf{Q}^n_{i+1})$ is a function of the left and the right state and still has to be chosen appropriately. For linear systems with constant coefficient matrix $\mathbf{A}$, the fluxes given by (2.8) & (2.3) and (2.10) are identical. For non-linear systems the two schemes provide almost coincident results, sa shown in Fig. (2.2) reporting the comparison between the results provided by the two schemes for the inviscid shallow water equations. The modified Lax-Wendroff-type flux (2.10) is introduced for technical reasons, in order to be able to prove later on that the proposed non-conservative centred schemes reduce exactly to the conservative centred scheme (2.5) with the modified FORCE flux (2.9), if the matrix $\mathbf{A}(\mathbf{Q})$ is the Jacobian of some flux function $\mathbf{F}(\mathbf{Q})$.

The PRICE-T scheme developed by Toro and Siviglia (2003), instead, consists of the following two steps:

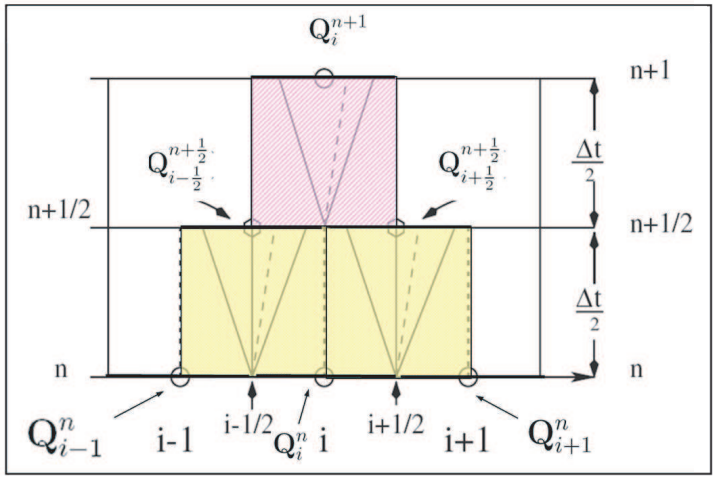

Figure 2.3: Sketch of the PRICE-T scheme of Toro and Siviglia (2003). The staggered grid at time $t = t^{n+1/2}$ is also shown.

- first step: computation of the intermediate state

$$\mathbf{Q}_{i+\frac{1}{2}}^{n+\frac{1}{2}} = \frac{1}{2}(\mathbf{Q}_i^n + \mathbf{Q}_{i+1}^n) - \frac{1}{2}\frac{\Delta t}{\Delta x}\widehat{\mathbf{A}}_{\mathbf{i+\frac{1}{2}}}\left[\mathbf{Q}_{i+1}^n - \mathbf{Q}_i^n\right] \ , \tag{2.11}$$

- second step: update formula

$$\mathbf{Q}_i^{n+1} = \frac{1}{2}\left(\mathbf{Q}_{i-\frac{1}{2}}^{n+\frac{1}{2}} + \mathbf{Q}_{i+\frac{1}{2}}^{n+\frac{1}{2}}\right) - \frac{1}{2}\frac{\Delta t}{\Delta x}\widehat{\mathbf{A}}_{\mathbf{i}}\left(\mathbf{Q}_{i+\frac{1}{2}}^{n+\frac{1}{2}} - \mathbf{Q}_{i-\frac{1}{2}}^{n+\frac{1}{2}}\right) \ . \tag{2.12}$$

where the matrices are evaluated as:

$$\widehat{\mathbf{A}}_{\mathbf{i}} = \mathbf{A}\left(\frac{1}{2}[\mathbf{Q}_{i-\frac{1}{2}}^{n+\frac{1}{2}} + \mathbf{Q}_{i+\frac{1}{2}}^{n+\frac{1}{2}}]\right) \ , \ \widehat{\mathbf{A}}_{\mathbf{i+\frac{1}{2}}} = \mathbf{A}\left(\frac{1}{2}[\mathbf{Q}_i^n + \mathbf{Q}_{i+1}^n]\right) \ . \tag{2.13}$$

The scheme was obtained integrating the PDE equations on the volume depicted in Fig.2.3. When applied to the linear model equation $\partial q/\partial t = \lambda \partial q/\partial x$, the PRICE-T scheme coincides with the FORCE scheme, that is first-order accurate, monotone and has linearized stability condition (Toro and Siviglia, 2003):

$$c = \lambda(\Delta t/\Delta x) \leq 1 \tag{2.14}$$

where c is the Courant-Friedrichs-Levy (CFL) number. The equality between the two schemes is not true for the case of nonlinear system of equations. It

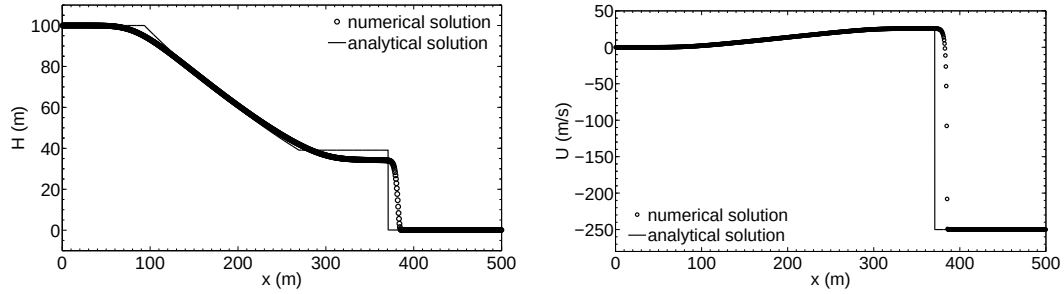

Figure 2.4: Dam break problem generating a strong shock wave (initial conditions $h_l = 100m$, $h_r = 0.1m$, $u_l = 0$ and $u_r = -250m/s$). Results after t =5 s obtained with the first-order PRICE-T scheme of Toro and Siviglia (2003) and compared with the exact solution (line). 1000 cells have been used.

was shown by Toro and Siviglia (2003) that for the shallow water equations the price-T scheme provides an acceptable error in the computation of the exact solution in presence of weak shocks. However, in the presence of a strong shock the scheme is unable to capture both the exact position of the front and the exact values of the conservative variables behind the shock (Fig. 2.4). In fact, Hou and LeFloch (1994) theorem proves that non-conservative methods will converge to the wrong solution in the presence of a shock wave.

Therefore the aim of this thesis, is to develop a modified PRICE-T scheme that degenerate to the FORCE scheme in case that $\mathbf{A}(\mathbf{Q})$ is the Jacobian matrix $\mathbf{A}(\mathbf{Q}) = \partial\mathbf{F}/\partial\mathbf{Q}$. The relevance of this result is noteworthy: it has been proved, in fact, that FORCE is the optimal centred scheme in the sense that it is the least dissipative of all three-point centred methods that are monotone and have stability condition (2.14) (see Toro and Billett, 2000, for details.) Furthermore, it will be shown that the proposed scheme preserves some particular equilibria of the governing PDE (well-balanced property) and should be easily extendable to high order of accuracy in space and time.

2.2.2 The PRICE-R scheme

The system (2.1) contains a nonconservative product $\mathbf{A}\partial\mathbf{Q}/\partial x$ which, in general, cannot make sense within the framework of the theory of distributions. With the theory developed by Dal Maso, LeFloch, and Murat (1995), a rigorous definition of weak solutions can be performed using a family of paths Φ in Ω. Once a family of paths is chosen it is possible to give a sense to the non-conservative product as a Borel measure (see Dal Maso et al. (1995) for details), denoted by $[\mathbf{A}\partial\mathbf{Q}/\partial x]_\Phi$ and weak solutions are the functions satisfying the equality $\partial\mathbf{Q}/\partial t + [\mathbf{A}\partial\mathbf{Q}/\partial x]_\Phi = 0$. Moreover, in Toumi (1992) a generalization of the Roe method to systems of the form (2.1) was introduced. Given a family of paths Ψ, a matrix $\mathbf{A}_\Psi$ is called a Roe linearization if it satisfies:

- for any $\mathbf{Q}_L, \mathbf{Q}_R \in \Omega$, $\mathbf{A}_\Psi(\mathbf{Q}_L, \mathbf{Q}_R)$ has N real distinct eigenvalues;
- $\mathbf{A}_\Psi(\mathbf{Q}, \mathbf{Q}) = \mathbf{A}(\mathbf{Q})$, for any $\mathbf{Q} \in \Omega$
- for any $\mathbf{Q}_L, \mathbf{Q}_R \in \Omega$:

$$\mathbf{A}_\Psi(\mathbf{Q}_L, \mathbf{Q}_R)(\mathbf{Q}_R - \mathbf{Q}_L) = \int_0^1 \mathbf{A}(\Psi(s, \mathbf{Q}_L, \mathbf{Q}_R))\frac{\partial \Psi}{\partial x} ds \tag{2.15}$$

If $\mathbf{A}(\mathbf{Q})$ is the Jacobian matrix of the flux $\mathbf{F}(\mathbf{Q})$, then (2.15) is independent of the choice of the family of the path and the classical Roe property:

$$\mathbf{A}(\mathbf{Q}_L, \mathbf{Q}_R)(\mathbf{Q}_R - \mathbf{Q}_L) = \mathbf{F}(\mathbf{Q}_R) - \mathbf{F}(\mathbf{Q}_L) \tag{2.16}$$

is obtained. We can now derive a modified version of the PRICE-T scheme, called PRICE-R, expressing the matrices $\mathbf{A}_i$ and $\mathbf{A}_{i+\frac{1}{2}}$ in equations (2.11) and (2.12) as

$$\widehat{\mathbf{A}}_{\mathbf{i}} = \mathbf{A}_{\mathbf{\Psi}}\left(\mathbf{Q}_{i-\frac{1}{2}}^{n+\frac{1}{2}}, \mathbf{Q}_{i+\frac{1}{2}}^{n+\frac{1}{2}}\right), \quad \widehat{\mathbf{A}}_{\mathbf{i+\frac{1}{2}}} = \mathbf{A}_{\mathbf{\Psi}}\left(\mathbf{Q}_i^n, \mathbf{Q}_{i+1}^n\right) . \tag{2.17}$$

Using algebraic manipulations and equation (2.16), it is easy to prove that the scheme (2.11) & (2.12) with (2.17) reduces to the original *conservative* FORCE scheme (2.5) with the original FORCE flux (2.6) with (2.7) and (2.8), if $\mathbf{A}(\mathbf{Q})$ is the Jacobian matrix of a flux $\mathbf{F}(\mathbf{Q})$.

It can be shown (Castro et al., 2006) that the best choice for Ψ would be $\Psi = \Phi$. In practice is difficult and computationally expensive to build numerical schemes with this choice of Ψ, and so in the follow the simpler family of linear path

$$\Psi(s, \mathbf{Q}_L, \mathbf{Q}_R) = \mathbf{Q}_L + s(\mathbf{Q}_R - \mathbf{Q}_L) \,, \tag{2.18}$$

is chosen, that coincides with the definition of nonconservative product proposed by Volpert (1967), and it is shown to give good results with upwind methods of the Roe-type (Castro et al., 2006).

The choice of the matrices (2.17) has the advantage that the resulting PRICE-R method becomes exactly conservative if applied to conservation laws. However, it has the obvious disadvantage that one needs to compute the Roe matrix, which may become very cumbersome or even impossible for complicated hyperbolic systems. Since a truly centred approach is sought, i.e. the scheme should not need any wave propagation information contained in the underlying governing PDE, thus avoiding the explicit computation of the Roe matrix. An alternative to the analytical computation of the Roe-type matrix $\mathbf{A}_{\mathbf{\Psi}}$ is to use definition (2.15) and the segment path (2.18), which yields

$$\mathbf{A}_{\mathbf{\Psi}}(\mathbf{Q}_L, \mathbf{Q}_R)(\mathbf{Q}_R - \mathbf{Q}_L) = \left(\int_0^1 \mathbf{A}(\mathbf{\Psi}(s, \mathbf{Q}_L, \mathbf{Q}_R)) ds \right) (\mathbf{Q}_R - \mathbf{Q}_L). \tag{2.19}$$

Hence, the following definition of the Roe matrix $\mathbf{A}_{\mathbf{\Psi}}$ in the case of a segment path is obtained:

$$\mathbf{A}_{\mathbf{\Psi}}(\mathbf{Q}_L, \mathbf{Q}_R) = \int_0^1 \mathbf{A}(\mathbf{\Psi}(s, \mathbf{Q}_L, \mathbf{Q}_R)) ds. \tag{2.20}$$

The exact conservation properties of the PRICE-R schemes described above is valid if the integral (2.20) is computed *exactly*. For complicated nonlinear hyperbolic systems, the exact computation of the integral may quickly become too cumbersome, so that a classical high order accurate Gaussian quadrature rules is here proposed to compute the right hand side of eqn. (2.20) numerically. Given an M-point Gaussian quadrature rule with weights ω_j and positions s_j

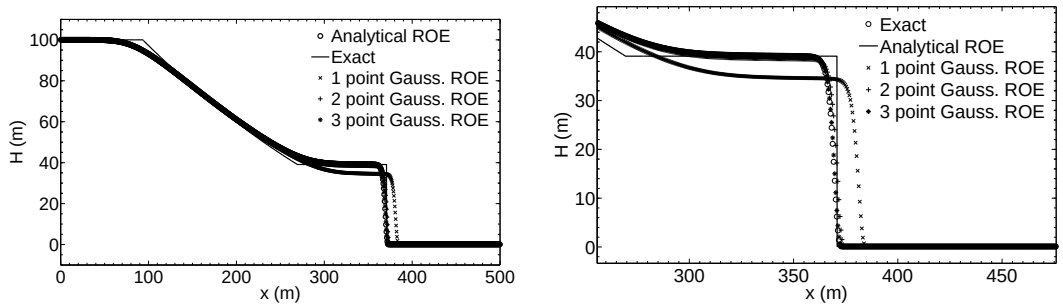

Figure 2.5: Inviscid dam break problem generating a strong shock wave (initial conditions $h_l = 100m$, $h_r = 0.1m$, $u_l = 0$ and $u_r = -250m/s$). The longitudinal distributions of the water surface elevation resulting from the first-order PRICE-R scheme using 1 to 3 Gaussian points (symbols) is plotted versus exact solution (line). The results refer to t =5 s and 1000 cells have been used. On the left it is shown the entire computational domain, while the right plot reports a zoom around the shock region.

distributed in the unit interval $[0; 1]$, a very accurate numerical approximation of the Roe matrix is:

$$\mathbf{A}_{\mathbf{\Psi}}(\mathbf{Q}_L, \mathbf{Q}_R) \approx \sum_{j=1}^{M} \omega_j \mathbf{A}(\mathbf{\Psi}(s_j, \mathbf{Q}_L, \mathbf{Q}_R)). \tag{2.21}$$

Recall that an M-point Gaussian quadrature rule integrates polynomials up to degree $2M - 1$ *exactly*, which means that *one* Gaussian point is enough if the system matrix $\mathbf{A}(\mathbf{Q})$ is a *linear function* in $\mathbf{Q}$. In order to study the sensitivity of the resulting PRICE-R scheme in association with the approximate Roe matrix (2.21) the behaviour of the method for the shallow water equations in presence of a strong shock wave is tested. The results are depicted in Fig. 2.5. The computations are carried out with different numbers of Gaussian points. It appears that with three or more Gaussian points the solution can not be distinguished any more from the solution obtained using the exact Roe matrix. So the basic idea of the present new scheme is to avoid the use of the analytical Roe matrix, which requires the knowledge of wave propagation information (*upwind philosophy*), and to use a Roe-type matrix which is computed numerically with a

number of Gaussian points that is adequate for the problem to be solved (*centred philosophy*). Moreover the reader can easily verify that the original PRICE-T scheme (2.11) and (2.12) with the matrices $\widehat{\mathbf{A}}_i$ and $\widehat{\mathbf{A}}_{i+\frac{1}{2}}$ given by (2.13) can be reinterpreted as the PRICE-R scheme, in which equation (2.21) is approximated with just one single Gaussian point. This choice was shown by Toro and Siviglia (2003) to give already reasonable shock-capturing properties in the case of weak shocks.

2.2.3 Alternative Formulation of the PRICE-R scheme

It is useful to observe that, after some easy algebra, equations (2.11) and (2.12) can be rewritten in the form:

$$\mathbf{Q}_i^{n+1} = \mathbf{Q}_i^n - \frac{\Delta t}{\Delta x}\left[\mathbf{A}^-_{i+\frac{1}{2}}(\mathbf{Q}_{i+1}^n - \mathbf{Q}_i^n) + \mathbf{A}^+_{i-\frac{1}{2}}(\mathbf{Q}_i^n - \mathbf{Q}_{i-1}^n)\right], \tag{2.22}$$

where

$$\mathbf{A}^-_{\mathbf{i+\frac{1}{2}}} = \frac{1}{4}\left[\widehat{\mathbf{A}}_{\mathbf{i}} - \frac{\Delta x}{\Delta t}\mathbf{I} + \widehat{\mathbf{A}}_{\mathbf{i+\frac{1}{2}}} - \frac{\Delta t}{\Delta x}\widehat{\mathbf{A}}_{\mathbf{i}}\widehat{\mathbf{A}}_{\mathbf{i+\frac{1}{2}}}\right] \tag{2.23}$$

and

$$\mathbf{A}^+_{\mathbf{i-\frac{1}{2}}} = \frac{1}{4}\left[\widehat{\mathbf{A}}_{\mathbf{i}} + \frac{\Delta x}{\Delta t}\mathbf{I} + \widehat{\mathbf{A}}_{\mathbf{i-\frac{1}{2}}} + \frac{\Delta t}{\Delta x}\widehat{\mathbf{A}}_{\mathbf{i}}\widehat{\mathbf{A}}_{\mathbf{i-\frac{1}{2}}}\right], \tag{2.24}$$

with $\mathbf{I}$ being the identity matrix and all matrices $\widehat{\mathbf{A}}$ computed as in (2.17). So the proposed scheme is thus recast in the same form of the path-conservative Roe scheme proposed in Parés (2006) and Castro et al. (2006; 2008b), the only difference being in the matrices $\mathbf{A}^-_{\mathbf{i+\frac{1}{2}}}$ and $\mathbf{A}^+_{\mathbf{i-\frac{1}{2}}}$. In the present formulation, these Roe-type matrices are centred, that is they do not use explicit wave properties information. Moreover, they are computed numerically, whereas in Castro et al. (2006; 2008b) they are computed as

$$\mathbf{A}^{\pm}_{\mathbf{i+\frac{1}{2}}} = \mathbf{A}_{\mathbf{\Psi}}\left(\mathbf{Q}_i^n, \mathbf{Q}_{i+1}^n\right)^{\pm} = \mathbf{R}_{\mathbf{\Psi}}\mathbf{\Lambda}^{\pm}_{\mathbf{\Psi}}\mathbf{R}^{-1}_{\mathbf{\Psi}}. \tag{2.25}$$

Here, the usual definitions apply, i.e. $\mathbf{R}_{\mathbf{\Psi}}$ is the matrix of right eigenvectors of the Roe matrix $\mathbf{A}_{\mathbf{\Psi}}$ and $\mathbf{\Lambda}_{\mathbf{\Psi}}$ is the diagonal matrix with the eigenvalues of $\mathbf{A}_{\mathbf{\Psi}}$. The matrices $\mathbf{\Lambda}^{\pm}_{\mathbf{\Psi}}$ are, as usual, either the positive or the negative part of the diagonal matrix $\mathbf{\Lambda}_{\mathbf{\Psi}}$.

2.2.4 The PRICE-C Scheme

The main drawback of the scheme (2.22),(2.23),(2.24) is that the matrices $\mathbf{A}^{+}_{\mathbf{i-\frac{1}{2}}}$ and $\mathbf{A}^{-}_{\mathbf{i+\frac{1}{2}}}$ are three-point functions, i.e. each of them depends on the *three* states $\mathbf{Q}^n_{i-1}$, $\mathbf{Q}^n_i$ and $\mathbf{Q}^n_{i+1}$. This prevents a direct extension of the PRICE-R method to multiple space dimensions and high order of accuracy using a polynomial reconstruction of $\mathbf{Q}$.

To circumvent this problem, it is here proposed to modify the matrices $\mathbf{A}^{+}_{\mathbf{i-\frac{1}{2}}}$ and $\mathbf{A}^{-}_{\mathbf{i+\frac{1}{2}}}$, substituting the matrix $\widehat{\mathbf{A}}_{\mathbf{i}}$ in (2.23) with $\widehat{\mathbf{A}}_{\mathbf{i+\frac{1}{2}}}$ and the matrix $\widehat{\mathbf{A}}_{\mathbf{i}}$ in (2.24) with $\widehat{\mathbf{A}}_{\mathbf{i-\frac{1}{2}}}$, in order to make them only two-point functions of the two adjacent states. After these modification, the final non-conservative version of the FORCE method, hereinafter called PRICE-C scheme , reads as follows:

$$\mathbf{Q}^{n+1}_i = \mathbf{Q}^n_i - \frac{\Delta t}{\Delta x}\left[\mathbf{A}^{-}_{i+\frac{1}{2}}(\mathbf{Q}^n_{i+1} - \mathbf{Q}^n_i) + \mathbf{A}^{+}_{i-\frac{1}{2}}(\mathbf{Q}^n_i - \mathbf{Q}^n_{i-1})\right], \tag{2.26}$$

with

$$\mathbf{A}^{-}_{\mathbf{i+\frac{1}{2}}} = \frac{1}{4}\left[2\mathbf{A}_{\mathbf{\Psi}}\left(\mathbf{Q}^n_i, \mathbf{Q}^n_{i+1}\right) - \frac{\Delta x}{\Delta t}\mathbf{I} - \frac{\Delta t}{\Delta x}\left(\mathbf{A}_{\mathbf{\Psi}}\left(\mathbf{Q}^n_i, \mathbf{Q}^n_{i+1}\right)\right)^2\right] \tag{2.27}$$

and

$$\mathbf{A}^{+}_{\mathbf{i-\frac{1}{2}}} = \frac{1}{4}\left[2\mathbf{A}_{\mathbf{\Psi}}\left(\mathbf{Q}^n_{i-1}, \mathbf{Q}^n_i\right) + \frac{\Delta x}{\Delta t}\mathbf{I} + \frac{\Delta t}{\Delta x}\left(\mathbf{A}_{\mathbf{\Psi}}\left(\mathbf{Q}^n_{i-1}, \mathbf{Q}^n_i\right)\right)^2\right]. \tag{2.28}$$

Now the matrices $\mathbf{A}^{-}_{\mathbf{i+\frac{1}{2}}}$ and $\mathbf{A}^{+}_{\mathbf{i-\frac{1}{2}}}$ only depend on two adjacent states. With the properties (2.20) and (2.16) it can be easily proven that if the PDE (2.1) is a conservation law (2.2), then:

$$\mathbf{A}^{-}_{\mathbf{i+\frac{1}{2}}}\left(\mathbf{Q}^n_{i+1} - \mathbf{Q}^n_i\right) = \mathbf{F}^{FORCE'}_{i+\frac{1}{2}} - \mathbf{F}(\mathbf{Q}^n_i), \tag{2.29}$$

$$\mathbf{A}^{+}_{\mathbf{i-\frac{1}{2}}}\left(\mathbf{Q}^n_i - \mathbf{Q}^n_{i-1}\right) = \mathbf{F}(\mathbf{Q}^n_i) - \mathbf{F}^{FORCE'}_{i-\frac{1}{2}}. \tag{2.30}$$

Therefore, the PRICE-C scheme (2.26)-(2.28) reduces to the modified conservative FORCE method (2.5), (2.9), (2.10) if $\mathbf{A}$ is the Jacobian of a flux $\mathbf{F}$.

It has to be emphasized that this new formulation has the important advantage that an explicit computation of the Roe averages is *not necessary*, following

the original philosophy of centred schemes that by definition do not need any additional information on the PDE system. At the same time conservation can be practically maintained up to any desired precision using Gaussian quadrature rules of appropriate order of accuracy. For complicated nonlinear PDE, as they typically arise in industrial, civil and environmental engineering, closed analytical expressions for the Roe averages may be impossible to obtain for a given PDE system. This will be shown later on, by applying the proposed PRICE-C scheme to the shallow water equations in the presence of movable bed using a complex closure relation for bed-load transport.

2.3 High Order Extension

2.3.1 Nonlinear Reconstruction Technique

This section discusses the proposed nonlinear weighted essentially non-oscillatory (WENO) procedure to reconstruct higher order polynomial data within each spatial cell $T_i = [x_{i-\frac{1}{2}}; x_{i+\frac{1}{2}}]$ at time t^n from the given cell averages $\mathbf{Q}_i^n$. It has to be noted that the reconstruction procedure is *nonlinear* and depends strongly on the input data $\mathbf{Q}_i^n$. Thus, the resulting numerical scheme, even when applied to a completely linear PDE, will be non-linear and thus it will not be possible to give a closed expression of the scheme. Indeed Godunov's theorem states that linear numerical schemes for solving partial differential equations, having the property of not generating new extrema (monotone scheme), can be at most first-order accurate. Therefore, if a non-oscillatory high-order scheme is sought, the scheme has to be non-linear.

The reconstruction procedure described here for the one-dimensional case follows directly from the guidelines given by Dumbser and Käser (2007) for general unstructured two- and three-dimensional meshes. It reconstructs *entire polynomials*, as the original ENO approach proposed by Harten et al. (1987). However, the method is here written as a WENO scheme (Jiang and Shu, 1996; Liu et al., 1994) with a particularly simple choice for the linear weights. The most impor-

tant difference of this approach compared to classical WENO schemes is that standard WENO methods reconstruct *point values* at the Gaussian integration points instead of an entire polynomial valid inside each element T_i.
Reconstruction is done for each element on a reconstruction stencil $\mathcal{S}_i^s$, given by the following union of the element T_i and its neighbors T_j,

$$\mathcal{S}_i^s = \bigcup_{j=i+s-k}^{i+s+k} T_j, \tag{2.31}$$

where s is the stencil shift with respect to the central element T_i and k is the spatial extension of the stencil to the left and the right. A central reconstruction stencil is given by $s = 0$, an entirely left-sided stencil is given by $s = -k$ and an entirely right-sided stencil is given by $s = k$. In the present approach it is always made use of the three fixed reconstruction stencils $\mathcal{S}_i^0$, $\mathcal{S}_i^{-k}$ and $\mathcal{S}_i^k$.
Given the cell average data $\mathbf{Q}_i^n$ in all elements T_i, a spatial reconstruction polynomial obtained from $\mathcal{S}_i^s$ at time t^n is seek in the form

$$\mathbf{w}_i^s(x, t^n) = \sum_{l=0}^{N} \Psi_l(x) \hat{\mathbf{w}}_l^{(i,s)}(t^n) := \Psi_l(x) \hat{\mathbf{w}}_l^{(i,s)}(t^n), \tag{2.32}$$

where the rescaled Legendre polynomials are used for the spatial reconstruction basis functions $\Psi_l(x)$ such that the $\Psi_l(x)$ form an orthogonal basis on the element T_i. In the following, standard tensor index notation is used, implying summation over indices appearing twice. The number of polynomial coefficients (degrees of freedom) is $L = N + 1$, where N is the degree of the reconstruction polynomial. To compute the reconstruction polynomial $\mathbf{w}_i(x, t^n)$ valid for element T_i integral conservation for all elements T_j inside the stencil $\mathcal{S}_i^s$ is required, i.e.

$$\frac{1}{\Delta x} \int_{T_j} \mathbf{w}_i^s(x, t^n) dx = \frac{1}{\Delta x} \int_{T_j} \Psi_l(x) dx \cdot \hat{\mathbf{w}}_l^{(i,s)}(t^n) = \mathbf{Q}_j^n, \qquad \forall T_j \in \mathcal{S}_i^s. \tag{2.33}$$

Equation (2.33) yields a linear equation system of the form

$$B_{jl} \cdot \hat{\mathbf{w}}_l^{(i,s)}(t^n) = \mathbf{Q}_j^n \tag{2.34}$$

for the unknown coefficients $\hat{\mathbf{w}}_l^{(i,s)}(t^n)$ of the reconstruction polynomial on stencil $\mathcal{S}_i^s$. Since $k = N/2$ is chosen for even N and $k = (N+1)/2$ is chosen for odd N, the number of elements in $\mathcal{S}_i^s$ may become larger than the number of degrees of freedom L. In this case, a constrained least-squares technique is used according to Dumbser and Käser (2007) to solve (2.34).

To obtain the final non-oscillatory reconstruction polynomials for each element T_i at time t^n, a data-dependent nonlinear combination of the polynomials $\mathbf{w}_i^0(x,t^n)$, $\mathbf{w}_i^{-k}(x,t^n)$ and $\mathbf{w}_i^k(x,t^n)$ obtained from the central, left-sided and right-sided stencils is finally constructed as follows:

$$\mathbf{w}_i(x,t^n) = \hat{\mathbf{w}}_l^i(t^n)\Psi_l(x), \tag{2.35}$$

with

$$\hat{\mathbf{w}}_l^i(t^n) = \omega_0\,\hat{\mathbf{w}}_l^{(i,0)}(t^n) + \omega_{-k}\,\hat{\mathbf{w}}_l^{(i,-k)}(t^n) + \omega_k\,\hat{\mathbf{w}}_l^{(i,k)}(t^n). \tag{2.36}$$

The nonlinear weights ω_s are given by the relations

$$\omega_s = \frac{\tilde{\omega}_s}{\tilde{\omega}_0 + \tilde{\omega}_{-k} + \tilde{\omega}_k}, \quad \tilde{\omega}_s = \frac{\lambda_s}{(\sigma_s + \epsilon)^r}. \tag{2.37}$$

In this particular formulation, the oscillation indicators σ_s are computed from

$$\sigma_s = \Sigma_{lm}\,\hat{\mathbf{w}}_l^s(t^n)\hat{\mathbf{w}}_m^s(t^n), \tag{2.38}$$

with

$$\Sigma_{lm} = \sum_{\alpha=1}^{N} \int_0^1 \Delta x^{2\alpha-1} \frac{\partial^\alpha \Psi_l(x)}{\partial x^\alpha} \cdot \frac{\partial^\alpha \Psi_m(x)}{\partial x^\alpha} dx. \tag{2.39}$$

Here, Σ_{lm} is the oscillation indicator matrix for element T_i. If all computations are done in a reference element, then this matrix does neither depend on the problem nor on the mesh, see Dumbser and Käser (2007). The parameters ϵ and r are constants and they are typically chosen as $\epsilon = 10^{-14}$ and $r = 8$. Moreover linear weights $\lambda_{-k} = \lambda_k = 1$ are chosen for $k \neq 0$, and a very large linear weight λ_0 is chosen on the central stencil, typically $\lambda_0 = 10^5$. It is worthwhile to observe that the numerical results are quite insensitive to the WENO parameters ϵ and r (Jiang and Shu, 1996; Liu et al., 1994) and also to the linear weight on the

central stencil λ_0, see Dumbser and Käser (2007).
The proposed reconstruction uses the accurate and linearly stable central stencil reconstruction in those regions of Ω where the solution is smooth because of the large linear weight λ_0. However, due to the strongly nonlinear dependence of the weights ω_s on the oscillation indicators σ_s, in the presence of discontinuities the smoother left- or right-sided stencils are preferred, as for standard ENO and WENO methods. For the nonlinear scalar case, the reconstruction operator described above can be directly applied to the cell averages $\mathbf{Q}_i^n$ of the conserved quantity $\mathbf{Q}$. For nonlinear hyperbolic systems, the reconstruction should be done in characteristic variables (Harten et al., 1987; Dumbser et al., 2007) in order to avoid spurious oscillations that may appear when applying ENO or WENO reconstruction operators component-wise to nonlinear hyperbolic systems.

2.3.2 High-Order Accurate One-Step Time Discretization

The result of the reconstruction procedure described in the previous section is a non-oscillatory spatial polynomial $\mathbf{w}_i(x,t^n)$ defined at time t^n inside each spatial element T_i. However, the temporal evolution of these polynomials inside each space-time element $[x_{i-\frac{1}{2}};x_{i+\frac{1}{2}}]\times[t^n;t^{n+1}]$ has to be computed in order to obtain the final high order accurate one-step finite volume scheme. To this purpose ADER approach of Toro and Titarev (2002) is used. The key idea therein being to solve, in a centred framework, high order Riemann problems at the element boundaries, this is accomplished by a Taylor series expansion in time and the use of the Cauchy-Kowalewski procedure. In this work the following strategy is adopted: local solution $\mathbf{Q}_i(x,t)$ of the PDE is expanded in each cell by a space-time Taylor series with respect to the element barycenter x_i

$$\begin{aligned}\mathbf{Q}_i(x,t) &= \mathbf{Q}(x_i,t^n)+(x-x_i)\frac{\partial\mathbf{Q}}{\partial x}+(t-t^n)\frac{\partial\mathbf{Q}}{\partial t}+\frac{1}{2}(x-x_i)^2\frac{\partial^2\mathbf{Q}}{\partial x^2}+\\ &\quad (x-x_i)(t-t^n)\frac{\partial^2\mathbf{Q}}{\partial t\partial x}+\frac{1}{2}(t-t^n)^2\frac{\partial^2\mathbf{Q}}{\partial t^2}+\ldots \qquad (2.40)\end{aligned}$$

where then the classical Cauchy-Kovalewski procedure is used in order to substitute time derivatives with space derivatives, using repeated differentiation of

the governing PDE system (2.1) with respect to space and time. In the following, the Cauchy-Kovalewski procedure is illustrated symbolically for third order of accuracy. For an efficient implementation up to any order of accuracy in space and time the reader is referred to Dumbser and Munz (2006) and Dumbser et al. (2007). For two more general and fully numerical alternatives to the semi-analytical Cauchy-Kovalewski procedure see Dumbser et al. (2008b) and Dumbser et al. (2008a), where local space-time finite element methods are used in order to compute the polynomial $\mathbf{Q}_i(x,t)$.

The first time derivative can be directly obtained from (2.1) as

$$\frac{\partial \mathbf{Q}}{\partial t} = -\mathbf{A}(\mathbf{Q})\frac{\partial \mathbf{Q}}{\partial x}. \tag{2.41}$$

The mixed space time derivative is then obtained after a differentiation with respect to space

$$\frac{\partial^2 \mathbf{Q}}{\partial t \partial x} = -\frac{\partial}{\partial x}\mathbf{A}(\mathbf{Q})\frac{\partial \mathbf{Q}}{\partial x} - \mathbf{A}(\mathbf{Q})\frac{\partial^2 \mathbf{Q}}{\partial x^2}, \tag{2.42}$$

and the second time derivative of $\mathbf{Q}$ is

$$\frac{\partial^2 \mathbf{Q}}{\partial t^2} = -\frac{\partial}{\partial t}\mathbf{A}(\mathbf{Q})\frac{\partial \mathbf{Q}}{\partial x} - \mathbf{A}(\mathbf{Q})\frac{\partial^2 \mathbf{Q}}{\partial t \partial x}. \tag{2.43}$$

The value of $\mathbf{Q}_i(x_i, t^n)$ and all purely spatial derivatives are obtained from the WENO reconstruction polynomial $\mathbf{w}_i(x, t^n)$.

2.3.3 The Fully Discrete High Order Accurate One-Step Scheme

Once the WENO reconstruction and the Cauchy-Kovalewski procedure have been performed for each cell, PDE (2.1) can be integrated over a space-time control volume $[x_{i-\frac{1}{2}}; x_{i+\frac{1}{2}}] \times [t^n; t^{n+1}]$ and the final high-order accurate one-step scheme can be written as:

$$\mathbf{Q}_i^{n+1} = \mathbf{Q}_i^n - \frac{1}{\Delta x}\mathbf{A}\mathbf{Q}_x - \frac{\Delta t}{\Delta x}\left[\mathbf{D}^-_{i+\frac{1}{2}} + \mathbf{D}^+_{i-\frac{1}{2}}\right], \tag{2.44}$$

where

$$\mathbf{AQ}_x = \int_{t^n}^{t^{n+1}} \int_{x^+_{i-\frac{1}{2}}}^{x^-_{i+\frac{1}{2}}} \mathbf{A}(\mathbf{Q}_i(x,t)) \frac{\partial}{\partial x} \mathbf{Q}_i(x,t) dx dt \tag{2.45}$$

and

$$\mathbf{D}^{\pm}_{i+\frac{1}{2}} = \frac{1}{\Delta t} \int_{t^n}^{t^{n+1}} \mathbf{A}^{\pm}_{i+\frac{1}{2}} \left(\mathbf{Q}^{+}_{i+\frac{1}{2}} - \mathbf{Q}^{-}_{i+\frac{1}{2}} \right) dt, \tag{2.46}$$

with

$$\mathbf{Q}^{-}_{i+\frac{1}{2}} = \mathbf{Q}_i(x_{i+\frac{1}{2}}, t) \qquad \text{and} \qquad \mathbf{Q}^{+}_{i+\frac{1}{2}} = \mathbf{Q}_{i+1}(x_{i+\frac{1}{2}}, t). \tag{2.47}$$

All the integrals are approximated using Gaussian quadrature formulae of suitable order of accuracy. Note that the term $\mathbf{AQ}_x$, which integrates the smooth part of the non-conservative product within each cell (excluding the jumps at the boundaries), vanishes for a first order scheme where $\frac{\partial}{\partial x}\mathbf{Q}_i(x,t) = 0$. The entire high-order one-step algorithm can be briefly summarized as follows:

1. Perform the WENO reconstruction described in section 2.3.1 in order to obtain the reconstruction polynomials $\mathbf{w}_i(x, t^n)$ for each cell.

2. Compute the spatial derivatives of $\mathbf{w}_i(x, t^n)$ and insert them into the Cauchy-Kovalewski procedure in order to get all missing space-time derivatives in the Taylor series (2.40). This step generates a space-time polynomial $\mathbf{Q}_i(x,t)$ for each cell T_i.

3. Use the space-time polynomials $\mathbf{Q}_i(x,t)$ together with Gaussian quadrature to compute the integrals appearing in the fully discrete scheme (2.44) and perform the update of the cell averages.

In the next chapter this high order algorithm is applied to the system of time-dependent non-linear shallow water equations with both fix and movable bed. The scheme is tested against both analytical solutions and real situations where experimental data are available.

Chapter 3

Application of the PRICE-C scheme to the one-dimensional shallow water equations

The PRICE-C scheme developed in the previous chapter is very general and it is applicable to any system of hyperbolic equations containing non-conservative products. In this chapter the performance of the developed high order algorithm is checked using as model system the time-dependent non-linear shallow water equations in the presence of either a fix or a movable bed.

The computations are carried out using second-order WENO polynomials, so that the resulting PRICE-C scheme is third order accurate in both time and space. The Courant number is set to CFL=0.9. The matrix (2.20) has been evaluated using a three-point Gaussian quadrature rule with the following points s_j and weights ω_j:

$$s_1 = \frac{1}{2}, \quad s_{2,3} = \frac{1}{2} \pm \frac{\sqrt{15}}{10}, \qquad \omega_1 = \frac{8}{18}, \quad \omega_{2,3} = \frac{5}{18}. \tag{3.1}$$

3.1 The fix bed case

The shallow water equations are the main tool for solving problems in hydraulic engineering, such as flood prediction in rivers and tide propagation in tidal channels. Here the system of equations with a geometrical source term due to the bed topography and in the absence of bottom friction is considered. The shallow water equations are analytically manipulated in order to use the water surface elevation, H, instead of the water depth, h, as a conservative variable. In one space dimension, the equations take the form:

$$\begin{cases} \frac{\partial H}{\partial t} + \frac{\partial q}{\partial x} = 0 \\ \frac{\partial q}{\partial t} + \frac{\partial}{\partial x}\left(\frac{q^2}{H-b} + \frac{1}{2}gH^2\right) + gH\frac{\partial b}{\partial x} = 0 \,, \end{cases} \tag{3.2}$$

where $H(x,t)$ denotes the water surface elevation, $q(x,t)$ is the discharge for unit width, $b(x)$ represents the given bottom topography and g is the gravity. System (3.2), together with the trivial equation $\frac{db}{dt} = 0$, can be written in the nonconservative form (2.1) with the vector $\mathbf{Q}$ and matrix $\mathbf{A}$ being respectively:

$$\mathbf{Q} = \begin{bmatrix} H \\ q \\ b \end{bmatrix} \quad , \quad \mathbf{A} = \begin{bmatrix} 0 & 1 & 0 \\ g(H-b) - \frac{q^2}{(H-b)^2} & \frac{2q}{H-b} & \frac{q^2}{(H-b)^2} \\ 0 & 0 & 0 \end{bmatrix} . \tag{3.3}$$

We note here that the scheme (2.44) with matrices (2.27) and (2.28) when applied to the shallow water equations produces an artificial motion of the bottom. In fact when the bottom is variable, the component (3,3) of the identity matrix $\mathbf{I}$ gives an undesirable diffusion that tends to flatten the bottom also if the water is quiescent. So in the follow we use a modified identity matrix $\mathbf{I}_m$ that reads:

$$\mathbf{I}_m = \begin{bmatrix} 1 & 0 & 0 \\ 0 & 1 & 0 \\ 0 & 0 & 0 \end{bmatrix} , \tag{3.4}$$

where the undesirable difussion of the bottom is eliminated. A number of different case studies are reported in the following. Each test case has been selected in order to verify a specific property of the scheme. Therefore, quiescent flow test cases are used to check the C-property achievement. Other tests are used to check the behaviour of the scheme in the case of a small perturbation of a quiescent state, a dam-break over a variable bottom profile and a steady flow over a smooth hump. An exact solution of the De Saint Venant-Exner equations is proposed to check the effective order of accuracy of the whole scheme. Finally the numerical model is compared with the experimental data obtained by Bellal et al. (2003) for an hydraulic jump over movable bed.

3.1.1 Verification of the C-property: still water

Algebraic Proof. It is well-known that numerical methods for the shallow water system with variable bottom must satisfy the so-called C-property as introduced by Bermudez and Vazquez (1994). It is evident that the governing equations contain non-vanishing terms also in the case of quiescent flow. Both the source term due to the bottom elevation $gH\partial b/\partial x$ and the flux term due to hydrostatic pressure $\frac{1}{2}gH^2$ are different from zero and the former balances the divergence of the latter. A scheme that satisfies the C-property has to be able to correctly solve this balance over any bottom profile, including discontinuous bottom.

For quiescent flow, we have $H = const.$, $u = 0$ and therefore

$$\Delta\mathbf{Q} = \begin{pmatrix} \Delta H \\ \Delta q \\ \Delta b \end{pmatrix} = \begin{pmatrix} 0 \\ 0 \\ \Delta b \end{pmatrix}, \qquad \mathbf{A}_\Psi = \begin{pmatrix} 0 & 1 & 0 \\ g\overline{h} & 0 & 0 \\ 0 & 0 & 0 \end{pmatrix}, \qquad \mathbf{A}_\Psi^2 = \begin{pmatrix} g\overline{h} & 0 & 0 \\ 0 & g\overline{h} & 0 \\ 0 & 0 & 0 \end{pmatrix}, \tag{3.5}$$

with $\overline{h} = \int_0^1 h(s)ds = \int_0^1 (h_L + s(h_R - h_L))ds$. Using the well-balanced identity matrix $\mathbf{I}_m$ it follows trivially from eqns. (2.26)-(2.28) and (3.4) that

$$\mathbf{A}^{\pm}_{i-\frac{1}{2}}\Delta\mathbf{Q} = 0 \tag{3.6}$$

and therefore the first order scheme verifies the exact C-property. Moreover also the term $\mathbf{AQ}_x$ in eqn. (2.44) vanishes, so also the higher order extensions satisfy the property.

Numerical verification. The aim of these simulations is now to verify whether also our actual implementation of the proposed PRICE-C scheme in computer code satisfies the *exact* C-property to machine precision. In order to verify this property we perform two different numerical experiments as as proposed in Xing and Shu (2006). In the first test case the bed elevation is smooth and is described by the Gaussian equation:

$$b(x) = 5e^{(-\frac{2}{5}(x-5)^2)} \ . \tag{3.7}$$

In the second test case the bed elevation is discontinuous and it is described by:

$$b(x) = \begin{cases} 4 \text{ m} & \text{if } 4 \leq x \leq 8 \text{ m} \\ 0 & \text{otherwise .} \end{cases} \tag{3.8}$$

The initial data for both the tests are the quiescent water solution:

$$H = h + b = 10 \text{ m} \quad , \quad q = 0 \ , \tag{3.9}$$

with h the water depth. Fig. 3.1 shows the initial conditions. To test the ability of the scheme to maintain the initial quiescent conditions, a simulation is carried out until $t = 5$ s, using a mesh of 200 cells, in a 10 m long domain. Table (3.1) shows that the property is exactly satisfied, the differences between the numerical solution and the reference solution being clearly due only to round-off errors.

3.1.2 A small perturbation of initially quiescent water

This test was first proposed by LeVeque (1998). It consists in the simulation of the convection of a small pulse in initially quiescent water. The bed topography consists in the following hump:

$$b(x) = \begin{cases} 0.25(\cos(10\pi(x - 1.5)) + 1) & \text{if } 1.4 \leq x \leq 1.6 \text{ m} \\ 0 & \text{otherwise} \end{cases} \tag{3.10}$$

Table 3.1: Verification of the C-property: water depth and specific discharge norms

Testcase	H (m)		q (m^2/s)	
	L_1	L_∞	L_1	L_∞
Test 1 (smooth)	3.25e-15	1.12e-14	2.42e-15	4.56e-14
Test 2 (non-smooth)	4.34e-15	1.45e-14	7.54e-15	3.23e-14

and the initial conditions are:

$$q(x,0) = 0 \qquad \text{and} \qquad H(x,0) = \begin{cases} 1+\epsilon & \text{if } 1.1 \leq x \leq 1.2 \text{ m} \\ 1 & \text{otherwise ,} \end{cases} \tag{3.11}$$

with ϵ a non-zero perturbation constant, chosen to be $\epsilon = 0.2$ m in the first test and $\epsilon = 0.001$ m in the second test. LeVeque (1998) showed that some numerical methods can give wrong solutions with the calculations involving such small perturbations of the water surface. The initial conditions are depicted in fig. 3.2, whereas the results for the water surface and the velocity are shown in fig. 3.3 and fig. 3.4. The solution obtained using the third order PRICE-C scheme with 400 cells is compared with a numerical reference solution obtained on a very

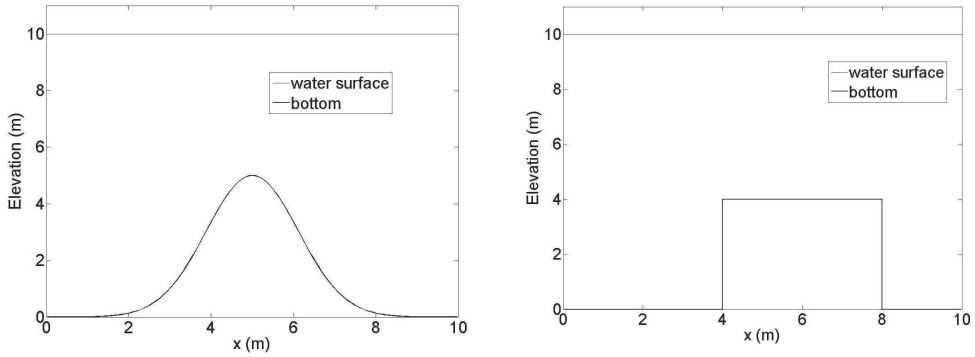

Figure 3.1: Verification of the C-property: initial conditions. On the left: smooth bottom. On the right: discontinuous bottom.

fine mesh with 3000 cells. No spurious oscillations are present in the solution. Moreover, the results are in good agreement with the results provided by Xing and Shu (2006, Figs. 3 and 5), with a fifth order TVD Runge-Kutta scheme. It has to be noted that in the second test, being $\epsilon/h << 1$, this disturbance should theoretically split into two waves, propagating left and right at the characteristic speed $\sqrt{gh}$, equal to 3.13 m/s. Therefore a wave should cover a distance of 0.626 m in 0.2 s. The position of the left front is in good agreement with the theoretical value $x = 1.1 - 0.626 = 0.474$ m. The right wave is a little bit slowed down with respect to the left wave, since it propagates over the hump, where $h < 1$.

Here the proposed scheme was shown to be able to compute correctly both a rapidly varying flow over a smooth bed and the perturbation of a stationary state.

3.1.3 Dam breaking over a rectangular hump

This test case was first introduced in Vukovic and Sopta (2002) and investigates the ability of the model to deal with a dam break over a discontinuous bottom.

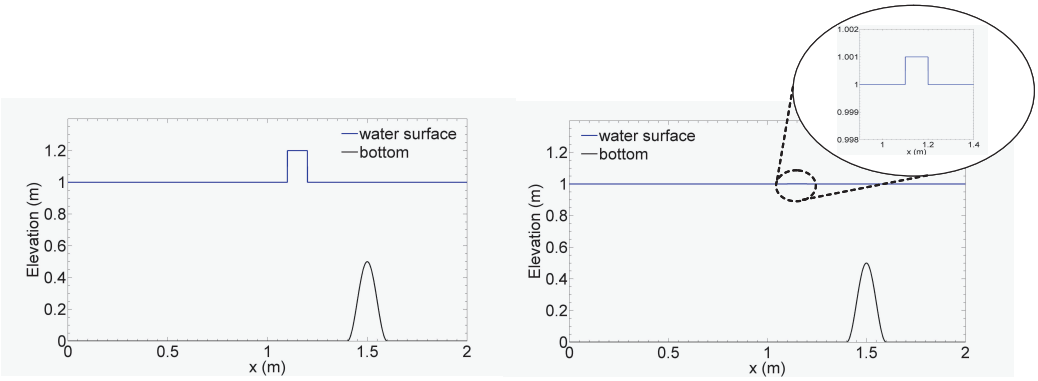

Figure 3.2: Small perturbation of initially quiescent water: initial conditions. On the left: $\epsilon = 0.2$ m. On the right: $\epsilon = 0.001$ m.

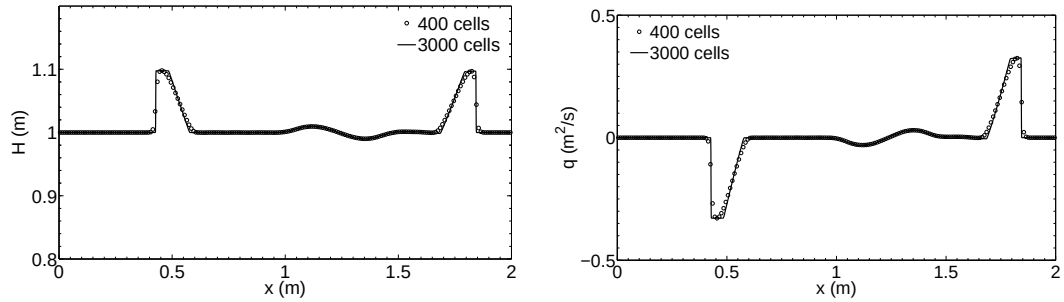

Figure 3.3: Small perturbation of initially quiescent water: $\epsilon = 0.2$ m. Results at time t =0.2 s for the third-order PRICE-C scheme with 400 cells (symbols) and with 3000 cells (line).

The bed surface is described by:

$$b(x) = \begin{cases} 8 & \text{if } |x - 750| \leq 1500/800 \text{ m} \\ 0 & \text{otherwise .} \end{cases} \tag{3.12}$$

The initial condition are:

$$q(x,0) = 0 \qquad \text{and} \qquad H(x,0) = \begin{cases} 20 \text{ m} & \text{if } x \leq 750 \text{ m} \\ 15 \text{ m} & \text{otherwise .} \end{cases} \tag{3.13}$$

Fig. 3.5 shows the initial conditions used in the test as well as the results after 15 and 60 sec. The solution obtained using 400 cells is compared to the solution

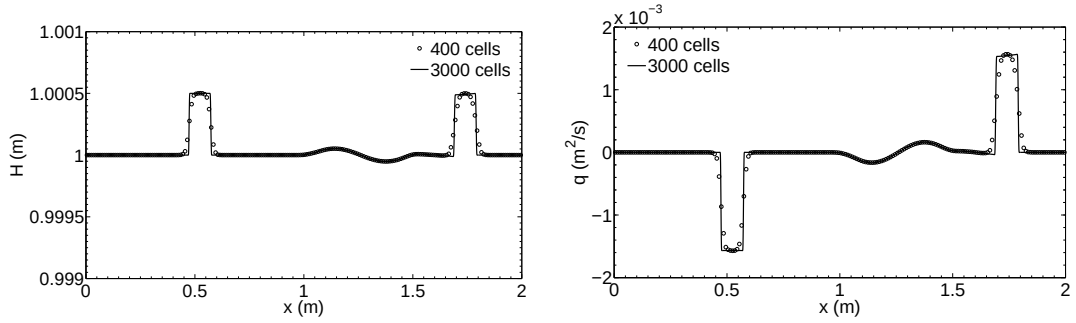

Figure 3.4: Small perturbation of a steady state water: $\epsilon = 0.001$ m. Results at time t =0.2 s for the third-order PRICE-C scheme with 400 cells (symbols) and with 3000 cells (line).

obtained using 4000 cells. No oscillations are generated neither at the bottom discontinuity nor at the surface shock. There is also a good agreement between the results provided by the coarse and the refined grid. Moreover the results agree with those provided by Xing and Shu (2006, Figs. 6 and 7) by using an high order TVD Runge-Kutta scheme.

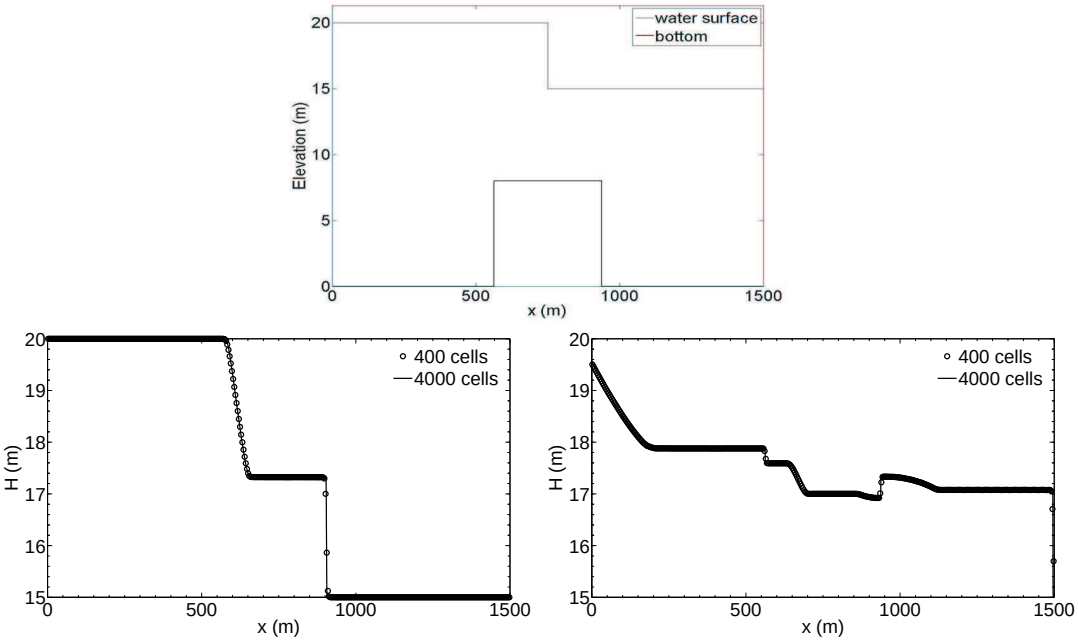

Figure 3.5: Dam breaking over a rectangular hump. On the top: initial conditions. On the bottom: spatial distribution of the water surface elevation computed through the third-order PRICE-C scheme with 400 cells (symbols) and with 4000 cells (line) is shown. On the left after $t = 15$ s. On the right after $t = 60$ s.

3.1.4 Steady flow over a smooth hump

The aim of these tests is to analyze the convergence in time towards a steady flow over a smooth bump. To this porpuse, three different tests (a, b, c) having exact solution are used. They have been proposed by the *Working group on dam*

break modeling (Goutal and Maurel, 1997). In the case of a steady flow, both the source term due to the bottom elevation, $gH\partial b/\partial x$, and the variation of the flux term, $\partial/\partial x \left[q^2/(H-b) + \frac{1}{2}gH^2\right]$, in (3.2) are different from zero, and the former has to balance the divergence of the latter. The bottom topography is described by:

$$b(x) = \begin{cases} 0.2 - 0.05(x-10)^2 & \text{if } 8 \leq x \leq 12 \text{ m} \\ 0 & \text{otherwise .} \end{cases} \tag{3.14}$$

The domain has a length of 25 m, and it is divided in 200 cells. Steady solutions have been obtained by marching in time, starting from an initial horizontal profile that is far away from the steady solution. The initial conditions are then taken as:

$$q(x,0) = 0 \qquad \text{and} \qquad H(x,0) = 0.5 \text{ m} .$$

several different configurations can be considered, characterized by smooth or discontinuous solutions, depending on the values of the water discharge Q, the maximum elevation of the bed profile and the boundary conditions for the free surface elevation. Three different cases are here considered. The bottom is the same for all of them and the different boundary conditions are summarized in Table 3.2. In test case (a) the steady solution is characterized by a transcritical

Table 3.2: Boundary conditions for the steady flow over a smooth hump

Test case	$q(x=0,t)$ [m^2/s]	$H(x=L,t)$ [m]
(a)	1.53	0.66
(b)	0.18	0.33
(c)	4.42	2.0

flow without a shock, in test (b) the solution is characterized by a transcritical flow with a shock, while in test (c) the solution is given by a completely subcritical flow. Analytical solutions for the various cases are computed following Goutal and Maurel (1997). The numerical and exact solutions for all test cases

are depicted in Fig. 4 at time $t = 200$ s. The agreement between the free surface elevation H computed numerically and analytically is excellent. Note the correct shock position and the good shock resolution for case (b). Moreover spurious oscillations are not produced at the discontinuity. The small errors that characterize the discharge are also present in other high order schemes documented in the literature, see e.g. Castro et al. (2006),since these errors are located where the cells include a discontinuity of the unknown variables or their derivatives.

3.2 Movable bed tests.

The system of equations that governs the transport of sediments in bed-load dominated rivers is obtained by coupling the shallow water equations (3.2) with an equation that describes the river bed evolution, namely the Exner equation. The latter reads:

$$\frac{\partial b}{\partial t} + \frac{\partial q_s}{\partial x} = 0, \tag{3.15}$$

where $b = b(x,t)$ is the movable bed elevation and q_s is the bedload sediment transport rate for unit width. Note that the porosity term is incorporated in q_s.For the quantification of q_s different relationships are available in literature. A simple power law formula (Grass, 1981), is used here for testing the method against exact analytical solutions, namely:

$$q_s = \frac{A(u-u_c)^m}{(1-\lambda_p)}, \tag{3.16}$$

where $u = q/(H-b)$ is the velocity of the water, u_c is the critical velocity below which the sediment transport vanishes, m is a positive exponent, and λ_p is the bed porosity. Other two empirical formulae available in literature have been also implemented. They are of the type:

$$q_s = \frac{\sqrt{(s-1)g d_s^3}}{(1-\lambda_p)} \Phi(\theta), \tag{3.17}$$

with s the relative density, and θ the local Shields stress given by

$$\theta = \frac{S_f h}{(s-1)d_s}, \tag{3.18}$$

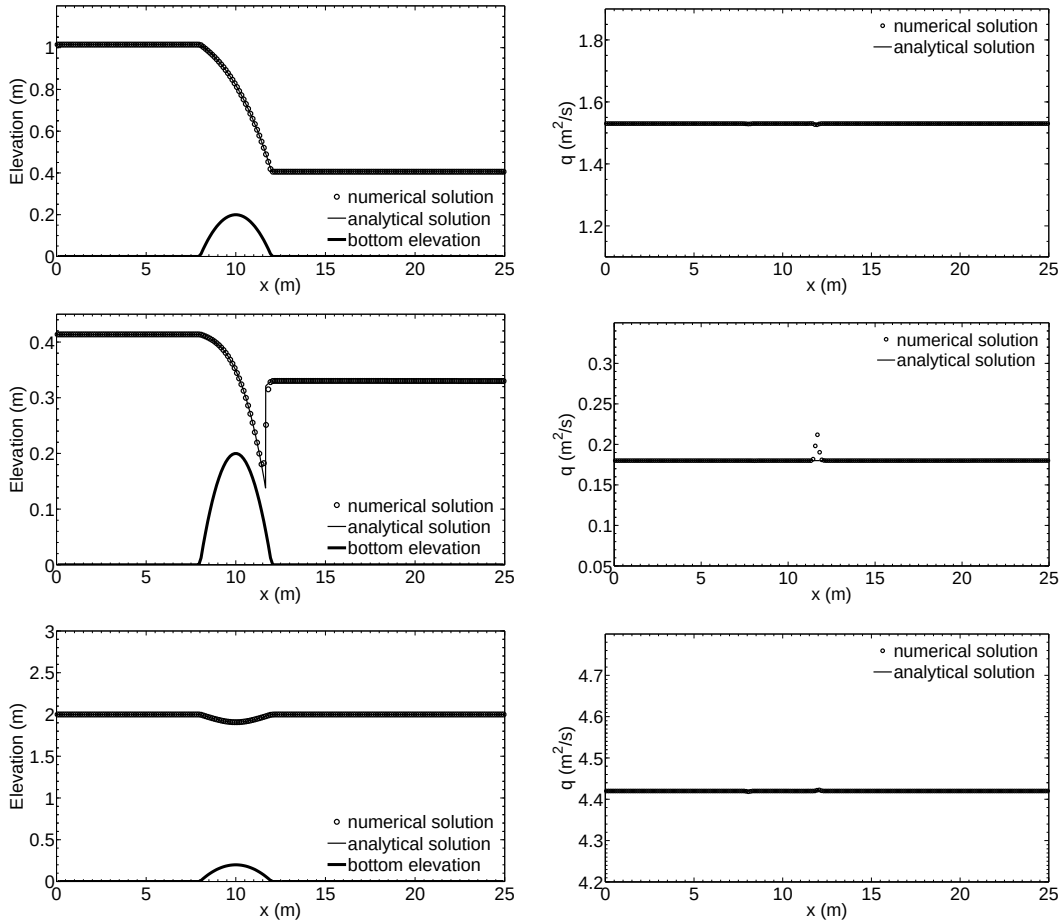

Figure 3.6: Steady flow over a smooth hump. Top row: test case (a). Middle row: test case (b). Bottom row: test case (c). The spatial distribution of the water surface elevation and the discharge per unit width are shown at time t =200 s. The third-order PRICE-C scheme is denoted by symbols while the exact solution is denoted by a line. 200 cells have been used.

.

d_s is the mean sediment diameter and S_f the friction term, calculated using the usual formula of Gauckler-Stricker. The sediment discharge function $\Phi(\theta)$ is evaluated on the basis of the formula proposed by either Parker (1990)

$$\Phi = 0.00218\ \theta^{3/2} G(\xi), \qquad \xi = \frac{\theta}{\theta_r}, \qquad \theta_r = 0.0386, \tag{3.19}$$

with

$$G = \begin{cases} 5474(1 - 0.853/\xi)^{4.5} & \xi \geq 1.59, \\ \exp\left[14.2(\xi - 1) - 9.28(\xi - 1)^2\right] & 1 \leq \xi \leq 1.59, \\ \xi^{14.2} & \xi < 1. \end{cases} \tag{3.20}$$

or Meyer-Peter and Müller (1948)

$$\Phi = 8(\theta - \theta_c)^{3/2}, \qquad \theta_c = 0.047. \tag{3.21}$$

It is worth noticing that the empirical nature of the relationships used to quantify the solid discharge q_s leads to the availability of a great number of different formulae, whose choice gives rise to a different system matrix $\mathbf{A}$ and, therefore, to a different formulation for the Roe matrix $\mathbf{A_\Psi}$. This would imply a huge effort when, as it usually occurs in practical applications, the various empirical formulations available in literature are tested in order to reproduce field measurements or laboratory experiments. The main advantage of the proposed PRICE-C method is that the fully numerical computation of the Roe matrix $\mathbf{A_\Psi}$ via Gaussian quadrature along the path completely avoids the need for an explicit computation of the Roe averages. Vukovic and Sopta (2002), for example, applied a WENO scheme to shallow water equations over movable bed by an upwind approach, but in this case only a very simple model for the sediment transport can be considered. On the other end the use of a central scheme permits the straightforward application of the methods to more complex, physically based, formulations.

The system of governing equations describing the coupled evolution of the fluid and the bed can be written in the form (2.1) with the vector $\mathbf{Q}$ and matrix $\mathbf{A}$ given by:

$$\mathbf{Q} = \begin{bmatrix} H \\ q \\ b \end{bmatrix} \quad , \quad \mathbf{A} = \begin{bmatrix} \frac{\partial q_s}{\partial H} & 1 + \frac{\partial q_s}{\partial q} & \frac{\partial q_s}{\partial b} \\ g(H-b) - \frac{q^2}{(H-b)^2} & \frac{2q}{H-b} & \frac{q^2}{(H-b)^2} \\ \frac{\partial q_s}{\partial H} & \frac{\partial q_s}{\partial q} & \frac{\partial q_s}{\partial b} \end{bmatrix}. \tag{3.22}$$

where $\partial q_s/\partial H$, $\partial q_s/\partial q$ and $\partial q_s/\partial b$ are the derivatives of the solid discharge with respect to the unknown variables. Note that the continuity equation of the fluid

has been changed to take into account the variability of the bed elevation. In the following the results provided by the proposed PRICE-C scheme are presented for three different test cases.

3.2.1 Numerical Convergence Study

An original exact solution is here derived for equations (2.1) with (3.22). If the following power law

$$q_s = aq^m \qquad \text{with} \qquad a = -(1-p) \quad , \quad m = 1 \; , \tag{3.23}$$

is chosen for the solid discharge, it can be easily verified that the functions $H(x,t)$, $Q(x,t)$ and $b(x,t)$ which satisfy exactly equations (3.2) and (3.15) are:

$$H(x,t) = 0 \qquad , \qquad q(x,t) = \frac{\omega}{\lambda} h_0 + a_0 \frac{\omega}{\lambda} sin(\lambda x - \omega t) \tag{3.24}$$

$$b(x,t) = -h(x,t) = -(h_0 + a_0 sin(\lambda x - \omega t)) \; , \tag{3.25}$$

with $\lambda = 2\pi/L$, $\omega = 2\pi/T$, λ and T being respectively the wave length and the period of the sinusoidal oscillation. Note the that the relationship (3.23) is not-physically based, but it allows one to find an exact solution by which the convergence rate of the numerical scheme can be tested. Periodical boundary conditions are prescribed in $x = 0$ and in $x = L$. Fig. 3.7 shows the results of the computations after 100 s. Table 3.3 shows the errors quantified through the standard norms L_1, L_∞ and relative convergence rates for variables h and q at the time $t = 10\,s$ with c_0=0.2 m , T_p = 1 s, L_w=10 m and using 100 cells. The expected orders of accuracy are achieved with each norm.

3.2.2 Propagation of a Small Sediment Hump Near Critical Conditions

The numerical scheme is now tested for a subcritical flow over a bump close to critical conditions. It has been shown by Sieben (1997; 1999) that for $Fr = u/\sqrt{gh}$ in the range $0.8 \div 1.2$, where $Fr = u/\sqrt{gh}$ is the Froude number, the

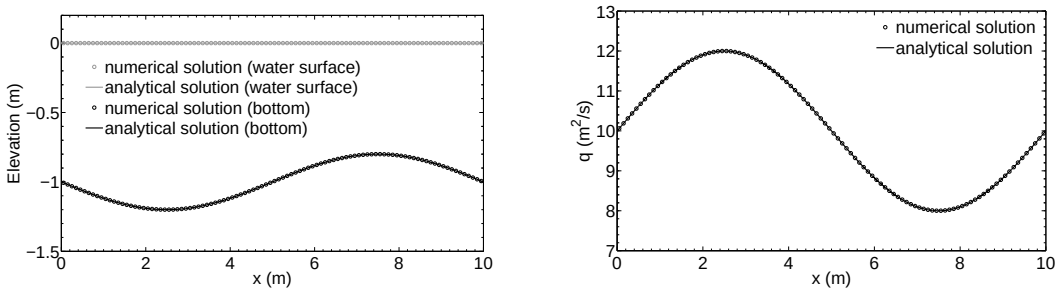

Figure 3.7: Convergence test with movable bed. Results are shown at time $t =$ 10 s using the third-order PRICE-C scheme with 100 cells (symbols) as well as the exact solution (line).

Table 3.3: Convergence rates study for the sediment transport problem with source terms for the third order PRICE-C method, (c_0=0.2 m , T_p = 1 s, L_w=10 m.)

	variable h				variable q			
N	L_1	$\mathcal{O}(L_1)$	L_∞	$\mathcal{O}(L_\infty)$	L_1	$\mathcal{O}(L_1)$	L_∞	$\mathcal{O}(L_\infty)$
20	5.54E-03		8.57E-03		1.39E-02		2.14E-02	
40	1.71E-03	1.70	2.70E-03	1.67	4.27E-03	1.70	6.75E-03	1.67
80	2.45E-04	2.80	3.86E-04	2.81	6.13E-04	2.80	9.64E-04	2.81
160	3.05E-05	3.01	4.79E-05	3.01	7.62E-05	3.01	1.20E-04	3.01
320	3.62E-06	3.08	5.68E-06	3.08	9.04E-06	3.08	1.42E-05	3.08
640	4.01E-07	3.17	6.30E-07	3.17	1.00E-06	3.17	1.57E-06	3.17

coupling between the shallow water equations and the Exner equation at each time step is crucial. In this range, in fact, each of the wave propagation celerities can no longer be identified solely with a surface wave or solely with a bed wave, and a full coupling of the equations is necessary to correctly solve the propagation of bed disturbances. Lyn and Altinakar (2002) found an exact solution of the linearized system:

$$\frac{\partial \mathbf{W}}{\partial t} + A\frac{\partial \mathbf{W}}{\partial x} = 0 \tag{3.26}$$

where:

$$\mathbf{W} = \begin{bmatrix} h \\ q \\ b \end{bmatrix} \quad , \quad \mathbf{A} = \begin{bmatrix} u_U & h_U & 0 \\ g & u_U & g \\ 0 & h_U\psi_U & 0 \end{bmatrix} \ , \tag{3.27}$$

the subfix U referring to the uniform unperturbed state, while ψ_U is a transport parameter defined by:

$$\psi_U = \frac{1}{(1-p)h_U}\frac{\partial q_s}{\partial x} \ . \tag{3.28}$$

This latter parameter is usually small for a wide range of physical problems, thus implying that the eigenstructure can be determined by a perturbation analysis near-critical conditions (i.e. $(1-Fr^2) = O(\psi_U^{1/2})$). The approximate expressions of the eigenvalues resulting from this analysis read (Lyn, 1987; Lyn and Altinakar, 2002):

$$\begin{aligned} \lambda_1 &= \left[\tfrac{3}{2} + \tfrac{1}{2Fr_U^2}\right] u_U \\ \lambda_{2,3} &= \left[\tfrac{1}{4}\left(1 - \tfrac{1}{Fr_U^2}\right) \pm \tfrac{1}{4}\sqrt{\left(1 - \tfrac{1}{Fr_U^2}\right)^2 + \tfrac{8\psi_U}{Fr_U^2}}\right] u_U \ , \end{aligned} \tag{3.29}$$

the corresponding left eigenvectors being $\mathbf{l}_i = [1, (\lambda_i - u_U)/g, 1 - u_U/\lambda_i]$. Denoting by $\mathbf{L}$ the matrix that has as rows the left eigenvectors and by $\mathbf{C} = \mathbf{LW}$ the vector of the characteristic variables, the analytical solution $\mathbf{W}(x,t)$ is provided by (Toro, 1999):

$$\mathbf{W}(x,t) = \mathbf{L}^{-1}\mathbf{C}^0(x - \lambda_i t) \ , \tag{3.30}$$

where $\mathbf{C}^0(x) = \mathbf{LW}^0(x)$ is the initial value of textbfC and $\mathbf{W}^0(x)$ the initial value of $\mathbf{W}$. In the present test computations are carried out with the following initial bed topography:

$$b(x,0) = b_{max}e^{-x^2} \qquad \text{with} \qquad -15\,\text{m} \le x \le 15\,\text{m} \ , \tag{3.31}$$

where $b_{max} = 10^{-5}$ m is the amplitude of the initial bed perturbation. Following Lyn and Altinakar (2002) we have set $Fr_U^2 = 0.96$ and $\psi_U = 2.5 \times 10^{-3}$. A water surface elevation corresponding to the water depth $h_U = 1$ m is prescribed downstream. A fixed-bed boundary condition is prescribed at the upstream and downstream ends of the computational domain, since the test is stopped before

the bed and water perturbations reach the domain boundaries. The upstream prescribed discharge is computed by using the values of h_U and Fr_U. The initial water surface for both the analytical and numerical solution is given respectively by the exact and the numerical solution obtained for a fixed bed (see the test described 3.1.4). The adopted grid spacing is $\Delta x = 0.02$m, leading to 500 cells. The following power-law sediment transport relationship (proposed by Phillips and Sutherland, 1989, for gravel flows) is chosen:

$$q_s = \beta(u - u_c)^r \ , \tag{3.32}$$

where $\beta = 3.4 \times 10^{-4}$ and $r = 2.65$. u_c is the critical velocity under which the sediment transport vanishes and it is calculated by (3.28) since the value of ψ_U is prescribed. Fig. 3.8 reports the comparison between the numerical and analytical results computed for $t = 20$ s. Water depth, flow discharge and bed elevation are plotted in non-dimensional form, the scaling parameters being:

$$h_{ref} = \frac{b_{max}}{(1 - Fr_U^2)} \quad ; \quad q_{ref} = u_U b_{max} \quad ; \quad b_{ref} = b_{max} \ . \tag{3.33}$$

The results show in a scour propagating upstream and a hump propagating downstream. In correspondence of the bottom disturbances the discharge presents an upstream travelling positive wave and a downstream travelling negative wave, while the water surface shows two negative waves. There is a good agreement between numerical and analytical solutions, and also with the results provided by other authors (see e.g. Lyn and Altinakar, 2002; Caleffi et al., 2007). These results then support the robustness of the scheme and his ability to deal with small disturbances of the bed elevation and the water level travelling in opposite directions.

3.2.3 Friction term discretization and comparison with laboratory results

In this section the friction term is introduced, so the scheme can be applied to real cases. The approach proposed by Gosse (2000) is used. Using the Gosse

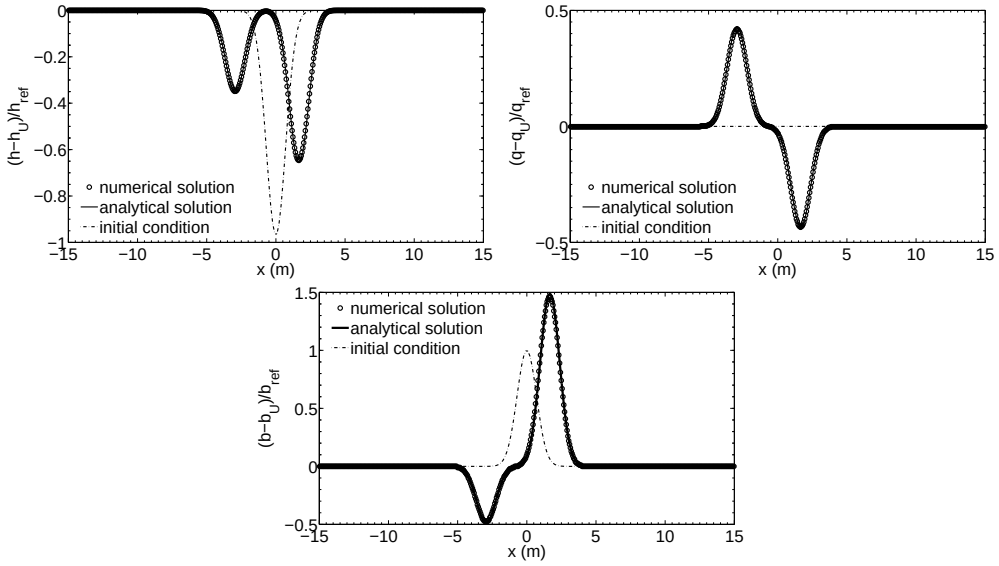

Figure 3.8: Propagation of a small sediment hump near critical conditions. Results at time t =20 s of the third-order PRICE-C scheme with 500 cells (symbols) and the exact solution (line). The initial conditions are also shown (dotted line).

approach allows to apply straightforwardly the presented PRICE-C scheme to the new system without any modifications. In fact, the approach consists in adding the trivial equation $\partial x/\partial t = 0$ to the original system. The following expressions for $\mathbf{Q}$ and $\mathbf{A}$ are thus obtained:

$$\mathbf{Q} = \begin{bmatrix} H \\ q \\ b \\ x \end{bmatrix}, \mathbf{A} = \begin{bmatrix} \frac{1}{(1-p)}\frac{\partial q_s}{\partial H} & 1 + \frac{1}{(1-p)}\frac{\partial q_s}{\partial q} & \frac{1}{(1-p)}\frac{\partial q_s}{\partial b} & 0 \\ g(H-b) - \frac{q^2}{(H-b)^2} & \frac{2q}{H-b} & \frac{q^2}{(H-b)^2} & g(H-b)S_f \\ \frac{1}{(1-p)}\frac{\partial q_s}{\partial H} & \frac{1}{(1-p)}\frac{\partial q_s}{\partial q} & \frac{1}{(1-p)}\frac{\partial q_s}{\partial b} & 0 \\ 0 & 0 & 0 & 0 \end{bmatrix}. \tag{3.34}$$

where S_f is the friction slope that is calculated, as usual, by an uniform flow formula. In this contribution the Gauckler-Stricker formula is used, giving $S_f = q^2/(R_h^{10/3}K_s^2)$, where R_h is the hydraulic radius, equal to $Bh/(2h+B)$ for a rectangular section having width B. In order to test the performance of the PRICE-C scheme we consider the flume experiment of Bellal et al. (2003). This experiment has been carried out in a steep-sloped, rectangular channel of finite length. The

bed profile was initially in quasi-equilibrium and a constant sediment supply was feed upstream. At the reference time t = 0, this equilibrium situation was perturbed by rapid raise of a submerged weir located at the downstream end of the flume, imposing a subcritical condition. The water and sediment discharges at the upstream section were kept constant. This new hydraulic configuration determined the formation of an hydraulic jump. In the first stage of the experiment, the hydraulic jump propagated rapidly upwards, with a negligible deposition of sediment, the transition time being very short. When the downstream water level was stabilised, the surge stopped its propagation. As the surge now remains steady, the sediments accumulated at this location creating a sediment bore. In the supercritical part of the flow, in fact, the sediments remained in motion, but not in the subcritical part, implying the sediments to depose at the transition. The continuous sediment supply from upstream progressively intensifies the bore amplitude forcing it to migrate downwards. In turn, the hydraulic jump slowly propagates downwards and decreases in amplitude.

The sudden increase of the downstream water level imposed in the experiment can occur in rivers due to an obstruction of the section or due to the presence of a check dam. The aggradational shock front caused by the presence of a transcritical flow represents a demanding test case for non-conservative scheme or conservative scheme with a wrong treatment of the slope and friction terms. These schemes, in fact, can fail in predicting both intensity and the propagation velocity of the front itself.

Run 2 of Bellal et al. (2003) is here considered for comparison purposes. The flume was 6.9 m long, 0.50 m wide and the slope was equal to 3.02% . The sediment and water discharge were respectively $Q_s = 0.136$ l/s and Q = 12 l/s. The induced water level at the downstream end was $H_0 = 20.93$ cm; uniform coarse sand with a mean diameter of 1.65mm, and porosity of 0.42 were used. Finally, Strickler bed roughness was $K_s = 60.60$ m$^{1/3}$s^{-1}.

Numerical simulations are conducted using the sediment transport formulae (3.19), (3.21) and a formula of the type (3.16) calibrated setting the parameters $A = 0.00024$, m=3 and $u_c = 0.3$ m/s. In fig. 3.9a the bottom and water surface

profiles obtained after 143 s using equation (3.21) are shown and compared with the experimental data. The position of the sediment bore obtained with the three different formulae is plotted in fig. 3.9b as a function of time and is compared with the experimental data of Bellal et al. (2003). The celerity of the front is given by the inverse of the slope of the above curves. The agreement between the experimental and numerical results is reasonably good. The model is able to capture the correct bed slope upstream of the bore, the height of the hydraulic jump and the height of the sediment bore. The celerity of propagation of the bore obviously depends on the transport formula which is used. Nevertheless, a good shock capturing method is here necessary to avoid a wrong estimate of front speed and strength thus yielding to an error which adds to the uncertainty of the sediment transport formula, providing totally meaningless results. Finally, it has to be noted that the physics of the hydraulic jump and the sediment bore is characterized by vertical velocities and turbulence that can not be modelled within a depth-averaged framework. Nevertheless, the main characteristics of the phenomenon are well-captured by the proposed one-dimensional model.

Concluding, it has to be highlighted the capability of the model to easily deal with not power-law bedload formulae. In the upwind approach of Castro et al. (2008b) the evaluation of the Roe matrix is needed. In the particular case of the power-law formula (or Grass model, see Grass (1981)) it is possible to determine analytically the Roe matrix when the family of paths is defined by segments. Nevertheless the calculus of the Roe matrices for the formulae here presented is not always possible in explicit form and its implementation is very costly. So the central approach here presented is very useful since it does not need the analytical expression of the Roe matrix.

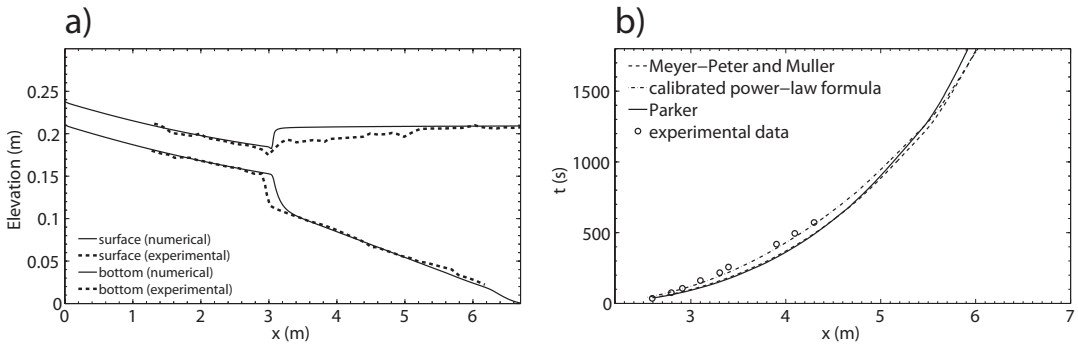

Figure 3.9: a) Comparison between experimental and numerical bottom and water surface profiles at $t = 143$ s. The Meyer-Peter Muller formula has been used. b) Comparison of front position using three different formulae for the quantification of the solid discharge. All the numerical computation are carried out with the third-order PRICE-C scheme

Chapter 4

Two-dimensional version of the PRICE-C scheme

This chapter concerns the extension of the one-dimensional PRICE-C scheme (2.26),(2.27),(2.28) described in chapter 2, to the two-dimensional case. Since the final aim is to build a numerical model that is able to deal with complex geometries, the scheme will be based on an unstructured mesh.

The extension to the two-dimensional case is not straightforward for centred schemes. As far the upwind schemes are concerned, once a one-dimensional flux is provided, the rotational invariance property of the two-dimensional equations is exploited to find a solution in a rotate system that is oriented normally to the element interfaces (see Toro, 1999; 2001). For the centred schemes usually this is not the case. In particular, using the one-dimensional FORCE flux (2.6) in a two-dimensional framework leads to an unstable scheme. Recently, a multi-dimensional extension of the FORCE scheme has been proposed in Toro et al. (2009). In this chapter a two-dimensional extension of the PRICE-C scheme (2.26),(2.27),(2.28) is found. It preserves the property of degenerating to the two-dimensional FORCE scheme if the underlying PDE system is a conservation law. Although the mathematical treatment provided in the following is in gen-

eral valid for the generic dimension α (=2,3), only two-dimensional applications will be exploited. In fact morphodynamic problems are seldom treated three-dimensionally, owing to the huge computational effort required by the analysis of real alluvial environmental.

4.1 Multi-dimensional non-conservative hyperbolic systems

Let us consider a system of hyperbolic partial differential equations in α space dimensions, written in the following form:

$$\frac{\partial \mathbf{Q}}{\partial t} + \underline{\underline{\mathbf{A}}}(\mathbf{Q}) \cdot \nabla \mathbf{Q} = \mathbf{0}, \qquad (\mathbf{x}, t) \in \mathbb{R}^{\alpha} \times \mathbb{R}_0^+, \qquad \mathbf{Q} \in \Omega \subseteq \mathbb{R}^N, \tag{4.1}$$

where $\mathbf{Q} = [q_1, \dots q_N]^T$ is the vector of unknowns and $\underline{\underline{\mathbf{A}}}(\mathbf{Q}) = (\mathbf{A}_1, \dots, \mathbf{A}_\alpha)$ is the vector of the coefficient matrices $\mathbf{A}_i = \mathbf{A}_i(\mathbf{Q})$, $i = 1, \dots, \alpha$, and a double underline denotes multi-dimensional vectors and matrices. As for the one-dimensional case, it is assumed that the unknown function $\mathbf{Q} = \mathbf{Q}(\mathbf{x}, t)$ takes its values inside an open convex set Ω included in $\mathbb{R}^N$ and that $\mathbf{Q} \to \underline{\underline{\mathbf{A}}}(\mathbf{Q})$ are smooth locally bounded map. The system (4.1) is assumed to be hyperbolic. Therefore, given an unit vector $\mathbf{n} = (n_1, \dots, n_\alpha) \in \mathbb{R}^\alpha$, the matrix

$$\mathbf{A}(\mathbf{Q}, \mathbf{n}) = \underline{\underline{\mathbf{A}}}(\mathbf{Q}) \cdot \mathbf{n} \tag{4.2}$$

is required to have N real eigenvalues $\lambda_1, \lambda_2, \dots \lambda_N$ and a full set of corresponding linearly independent right eigenvectors $\mathbf{r}_1, \mathbf{r}_2, \dots, \mathbf{r}_N$, $\forall \mathbf{Q} \in \Omega$ and $\forall \mathbf{n} \in \mathbb{R}^\alpha$. The vector of unknowns $\mathbf{Q}$ in (4.1) will be always chosen to be the vector of physically conserved variables. In the case that $\underline{\underline{\mathbf{A}}}(\mathbf{Q})$ is the Jacobian matrix $\underline{\underline{\mathbf{A}}}(\mathbf{Q}) = \partial \underline{\underline{\mathbf{F}}} / \partial \mathbf{Q}$ of some flux function $\underline{\underline{\mathbf{F}}} = (\mathbf{F}_1(\mathbf{Q}), \dots, \mathbf{F}_\alpha(\mathbf{Q}))$, the non-conservative system (4.1) can then be expressed in conservative form

$$\frac{\partial \mathbf{Q}}{\partial t} + \frac{\partial \underline{\underline{\mathbf{F}}}}{\partial x} = 0. \tag{4.3}$$

4.1.1 The FORCE Scheme for Multi-Dimensional Conservative Systems

Let us preliminarly recall the FORCE scheme for multi-dimensional conservation laws developed by Toro et al. (2009). Consider a conforming tesselation $\mathcal{T}_\Omega$ of the computational domain $\mathcal{T}_\Omega \subseteq R^\alpha$ by elements T_i:

$$T_\Omega = \bigcup_i T_i \, . \tag{4.4}$$

Each element T_i has n_f plane faces ∂T_i^j of area S_j with associated outward pointing face normal vectors $\mathbf{n}_j$. The total volume $|T_i|$ of element T_i is subdivided into sub-volumes generated by connecting the barycentre of element T_i with the vertex of face j. The corresponding adjacent sub-volume in the neighbouring element that shares the face ∂T_i^j with element T_i, is denoted as V_j^+. Fig 4.1 shows the configuration for the two-dimensional case. Integrating equations (4.3) in the volume $V_j^- \cup V_j^+$ between $t = 0$ and $t = \Delta t/2$, and then integrating in T_i between $t = \Delta t/2$ and $t = \Delta t$ the following scheme is obtained

$$\mathbf{Q}_{j+\frac{1}{2}}^{n+\frac{1}{2}} = \frac{\mathbf{Q}_i^n V_j^- + \mathbf{Q}_j^n V_j^+}{V_j^+ + V_j^-} - \frac{1}{2}\frac{\Delta t S_j}{V_j^+ + V_j^-}\left(\underline{\underline{\mathbf{F}}}(\mathbf{Q}_j^n) - \underline{\underline{\mathbf{F}}}(\mathbf{Q}_i^n)\right)\cdot \mathbf{n}_j, \tag{4.5}$$

$$\mathbf{Q}_i^{n+1} = \frac{1}{|T_i|}\sum_{j=1}^{n_f}\left(\mathbf{Q}_{j+\frac{1}{2}}^{n+\frac{1}{2}} - \frac{1}{2}\Delta t S_j \underline{\underline{\mathbf{F}}}(\mathbf{Q}_{j+\frac{1}{2}}^{n+\frac{1}{2}})\cdot \mathbf{n}_j\right), \tag{4.6}$$

or, using the more convenient conservative non-staggered one-step formulation:

$$\mathbf{Q}_i^{n+1} = \mathbf{Q}_i^n - \frac{\Delta t}{|T_i|}\sum_{j=1}^{n_f} S_j \underline{\underline{\mathbf{F}}}_{j+\frac{1}{2}}^{FORCE\alpha}\cdot \mathbf{n}_j \, , \tag{4.7}$$

where the $FORCE\alpha$ flux $\underline{\underline{\mathbf{F}}}_{j+\frac{1}{2}}^{FORCE\alpha}$ reads:

$$\underline{\underline{\mathbf{F}}}_{j+\frac{1}{2}}^{FORCE\alpha} = \frac{1}{2}\left(\underline{\underline{\mathbf{F}}}_{j+\frac{1}{2}}^{LF\alpha} + \underline{\underline{\mathbf{F}}}_{j+\frac{1}{2}}^{LW\alpha}\right). \tag{4.8}$$

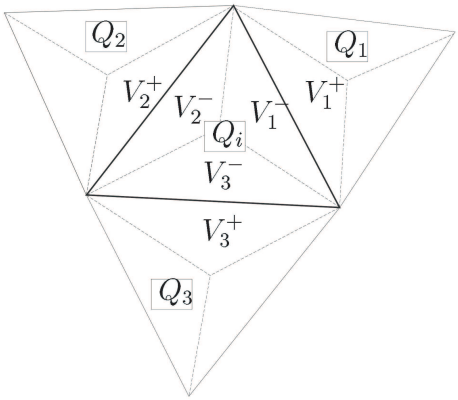

Figure 4.1: Notation of the general configuration on an unstructured two-dimensional triangolar mesh.

It then turns out that on general meshes in multiple space dimensions the $FORCE\alpha$ flux is the arithmetic average of the multi-dimensional generalization of the Lax-Friedrichs and Lax-Wendroff fluxes, reading, respectively:

$$\underline{\underline{\mathbf{F}}}^{LF\alpha}_{j+\frac{1}{2}} = \frac{V_j^- \underline{\underline{\mathbf{F}}}(\mathbf{Q}_j^n) + V_j^+ \underline{\underline{\mathbf{F}}}(\mathbf{Q}_i^n)}{V_j^- + V_j^-} - \frac{V_j^+ V_j^-}{V_j^+ + V_j^-} \frac{2}{\Delta t S_j} \left(\mathbf{Q}_j^n - \mathbf{Q}_i^n\right) \cdot \mathbf{n}_j^T, \tag{4.9}$$

$$\underline{\underline{\mathbf{F}}}^{LW\alpha}_{j+\frac{1}{2}} = \underline{\underline{\mathbf{F}}}\left(\mathbf{Q}^{n+\frac{1}{2}}_{j+\frac{1}{2}}\right), \tag{4.10}$$

with $\mathbf{Q}^{n+\frac{1}{2}}_{j+\frac{1}{2}}$ given by (4.5). It is easy to prove via simple algebraic manipulations that the two schemes (4.5) & (4.6) and (4.7) are identical. As for the one-dimensional case, the Lax-Wendroff as given in (4.5) and (4.10), is not convenient, due to the non-linearity of the numerical flux function with respect to the arguments $\mathbf{Q}_i^n$, $\mathbf{Q}_j^n$, $\underline{\underline{\mathbf{F}}}(\mathbf{Q}_i^n)$ and $\underline{\underline{\mathbf{F}}}(\mathbf{Q}_j^n)$. The following variant of the conservative $FORCE\alpha$ flux is then introduced here:

$$\underline{\underline{\mathbf{F}}}^{FORCE\alpha'}_{j+\frac{1}{2}} = \frac{1}{2}\left(\underline{\underline{\mathbf{F}}}^{LF}_{j+\frac{1}{2}} + \underline{\underline{\mathbf{F}}}^{LW'}_{j+\frac{1}{2}}\right), \tag{4.11}$$

where the modified Lax-Wendroff-type flux is now given by

$$\underline{\underline{\mathbf{F}}}^{LW'}_{j+\frac{1}{2}} = \frac{V_j^+ \underline{\underline{\mathbf{F}}}(\mathbf{Q}_j^n) + V_j^- \underline{\underline{\mathbf{F}}}(\mathbf{Q}_i^n)}{V_j^- + V_j^-} - \frac{1}{2}\frac{\Delta t}{\Delta x} \widehat{\mathbf{A}}_{j+\frac{1}{2}} \left(\underline{\underline{\mathbf{F}}}(\mathbf{Q}_j^n) - \underline{\underline{\mathbf{F}}}(\mathbf{Q}_i^n)\right). \tag{4.12}$$

The matrix $\widehat{\mathbf{A}}_{j+\frac{1}{2}} = \widehat{\mathbf{A}}_{j+\frac{1}{2}}(\mathbf{Q}_i^n, \mathbf{Q}_j^n)$ is a function of the two adjacent states and still has to be chosen appropriately. Note that for linear systems with constant coefficient matrix $\mathbf{A}$, the fluxes given by (4.5) & (4.10) and (4.12) are identical. It will be demonstrated later on that introducing the modified Lax-Wendroff-type flux (4.12) the proposed non-conservative centred schemes reduce exactly to the conservative centred scheme (4.7) with the modified FORCE flux given by (4.11), if the matrix $\underline{\underline{\mathbf{A}}}(\mathbf{Q})$ is the Jacobian of some flux function $\underline{\underline{\mathbf{F}}}(\mathbf{Q})$.

4.1.2 The Multidimensional PRICE-T Scheme

In this section the multi-dimensional version of the PRICE-T scheme, hereafter denoted by PRICEα-T, is derived. Integrating the non-conservative system (4.1) over the volume $V_j^- \cup V_j^+$ from $t = 0$ to $t = \Delta t/2$, and then integrating in T_i from $t = \Delta t/2$ to $t = \Delta t$ the following two-step scheme is obtained:

$$\mathbf{Q}_{j+\frac{1}{2}}^{n+\frac{1}{2}} = \frac{\mathbf{Q}_i^n V_j^- + \mathbf{Q}_j^n V_j^+}{V_j^+ + V_j^-} - \frac{1}{2}\frac{\Delta t S_j}{V_j^+ + V_j^-}\widehat{\mathbf{A}}_{j+\frac{1}{2}}(\mathbf{Q}_j^{\mathbf{n}}, \mathbf{Q}_i^n)(\mathbf{Q}_j^n - \mathbf{Q}_i^n), \tag{4.13}$$

$$\mathbf{Q}_i^{n+1} = \frac{1}{|T_i|}\sum_{j=1}^{n_f} \mathbf{Q}_{j+\frac{1}{2}}^{n+\frac{1}{2}} - \frac{\Delta t}{2\,|T_i|}\sum_{j=1}^{n_f} S_j \mathbf{A}_i \mathbf{Q}_{\mathbf{j+\frac{1}{2}}}^{\mathbf{n+\frac{1}{2}}}, \tag{4.14}$$

with $\widehat{\mathbf{A}}_{j+\frac{1}{2}}(\mathbf{Q}_i^n, \mathbf{Q}_j^n, \mathbf{n}) = \underline{\underline{\mathbf{A}}}_{j+\frac{1}{2}} \cdot \mathbf{n}_j$ and $\widehat{\mathbf{A}}_i(\mathbf{Q}_i^n, \mathbf{Q}_j^n, \ldots, \mathbf{Q}_{n_f}^n, \mathbf{n}) = \underline{\underline{\mathbf{A}}}_i \cdot \mathbf{n}_j$ two particular linearization of the matrix $\mathbf{A}(\mathbf{Q}, \mathbf{n})$ appearing in equation (4.2). This implies that also for the multi-dimensional case a modified PRICE-T scheme is sought that *automatically* reduces to the modified *conservative* FORCE scheme (4.11) when $\underline{\underline{\mathbf{A}}}(\mathbf{Q})$ is the multi-dimesional Jacobian matrix of some flux function $\underline{\underline{\mathbf{F}}}(\mathbf{Q})$ (i.e. $\underline{\underline{\mathbf{A}}}(\mathbf{Q}) = \partial\underline{\underline{\mathbf{F}}}/\partial\mathbf{Q}$).

4.1.3 Alternative Formulation of the PRICEα-T Scheme: the PRICEα-C scheme

After some algebraic manipulations, the two-step PRICEα-T scheme given by (4.13) and (4.14) can be rewritten as the one-step scheme

$$\mathbf{Q}_i^{n+1} = \mathbf{Q}_i^n - \frac{\Delta t}{|T_i|} \sum_{j=1}^{n_f} S_j \mathbf{A}_{ij}^- (\mathbf{Q}_j^n - \mathbf{Q}_i^n), \tag{4.15}$$

where

$$\begin{aligned} \mathbf{A}_{ij}^- \;=\; & \frac{1}{2} \frac{V_j^-}{V_j^+ + V_j^-} \widehat{\mathbf{A}}_{j+\frac{1}{2}} + \frac{1}{2} \frac{V_j^+}{V_j^+ + V_j^-} \widehat{\mathbf{A}}_i - \frac{V_j^+ V_j^-}{V_j^+ + V_j^-} \frac{1}{\Delta t S_j} \mathbf{I} + \\ & - \frac{1}{4} \frac{\Delta t S_j}{V_j^+ + V_j^-} \widehat{\mathbf{A}}_{j+\frac{1}{2}} \widehat{\mathbf{A}}_i \end{aligned} \tag{4.16}$$

with $\mathbf{I}$ the identity matrix. The main drawback of the formulation given by (4.15) and (4.16) is that the matrix $\widehat{\mathbf{A}}_i$ is a function of more then two states, thus preventing a direct extension of the PRICEα-T method to high order of accuracy through a polynomial reconstruction of $\mathbf{Q}$. In order to eliminate this shortcoming matrix $\widehat{\mathbf{A}}_i$ is here computed considering a different value $\widehat{\mathbf{A}}_{j+\frac{1}{2}}$ for each edge j, so that the matrix $\mathbf{A}_{ij}^-$ becomes a two-point function of the two adjacent states. After these modification, the final non-conservative version of the multi-dimensional FORCEα method, denoted as PRICEα-C reads:

$$\mathbf{A}_{ij}^- = \frac{1}{2} \widehat{\mathbf{A}}_{j+\frac{1}{2}} - \frac{V_j^+ V_j^-}{V_j^+ + V_j^-} \frac{1}{\Delta t S_j} \mathbf{I} - \frac{1}{4} \frac{\Delta t S_j}{V_j^+ + V_j^-} \widehat{\mathbf{A}}_{j+\frac{1}{2}}^2 \tag{4.17}$$

where the matrix $\mathbf{A}_{ij}^-$ only depends on two adjacent states. In the next paragraph the matrices $\widehat{\mathbf{A}}_{j+\frac{1}{2}}$ will be chosen requiring that the scheme (4.16) degenerates to the modified $FORCE\alpha$ scheme (4.11).

4.1.4 Generalized Roe matrix in the multidimensional case

Following the theory developed by Dal Maso et al. (1995), a rigorous definition of weak solutions in presence of non-conservative products can be given also in the

multi-dimensional case using a family of paths $\mathbf{\Psi} = \mathbf{\Psi}(\mathbf{Q_L}, \mathbf{Q_R}, s, \mathbf{n})$ connecting two states $\mathbf{Q_L}$ and $\mathbf{Q_R}$ across a discontinuity with ($s \in [0, 1]$). Given a family of paths $\mathbf{\Psi}$, a matrix $\mathbf{A_\Psi}(\mathbf{Q}_L, \mathbf{Q}_R, \mathbf{n})$ is a Roe matrix if it satisfies the following properties:

- for any $\mathbf{Q}_L, \mathbf{Q}_R \in \Omega$, $\mathbf{n} \in S^1$ (where $S^1 \subseteq R^\alpha$ denotes the unit sphere), $\mathbf{A_\Psi}(\mathbf{Q}_L, \mathbf{Q}_R, \mathbf{n})$ has N real distinct eigenvalues;
- $\mathbf{A_\Psi}(\mathbf{Q}, \mathbf{Q}, \mathbf{n}) = \mathbf{A}(\mathbf{Q}, \mathbf{n})$, for any $\mathbf{Q} \in \Omega$, $\mathbf{n} \in S^1$;
- for any $\mathbf{Q}_L, \mathbf{Q}_R \in \Omega$, $\mathbf{n} \in S^1$:

$$\mathbf{A_\Psi}(\mathbf{Q}_L, \mathbf{Q}_R, \mathbf{n})(\mathbf{Q}_R - \mathbf{Q}_L) = \int_0^1 \mathbf{A}(\mathbf{\Psi}(s, \mathbf{Q}_L, \mathbf{Q}_R, \mathbf{n}), \mathbf{n}) \frac{\partial \mathbf{\Psi}}{\partial s} ds. \tag{4.18}$$

thus implying that the multi-dimensional Roe matrix dipends on $\mathbf{n}$. Note also that when $\mathbf{A}_i(\mathbf{Q}), i = 1, \ldots, \alpha$ are the Jacobian matrices of smooth flux functions $\mathbf{F}_i(\mathbf{Q}), i = 1, \ldots, \alpha$, the relation (4.18) is independent of the family of paths and it reduces to the usual Roe property:

$$\mathbf{A_\Psi}(\mathbf{Q}_L, \mathbf{Q}_R, \mathbf{n})(\mathbf{Q}_R - \mathbf{Q}_L) = \mathbf{F_n}(\mathbf{Q}_R) - \mathbf{F_n}(\mathbf{Q}_L). \tag{4.19}$$

for any $\mathbf{n} = (n_1, \ldots, n_\alpha) \in S^1$, $\mathbf{F_n}(\mathbf{Q}) = \mathbf{F}_1 n_1 \ldots + \mathbf{F}_\alpha n_\alpha$ being the flux along the direction $\mathbf{n}$. If the system (4.1) is supposed to be rotationally invariant, the dependency of the family of paths on $\mathbf{n}$ disappears (Dal Maso et al., 1995).

The matrices $\widehat{\mathbf{A}}_{j+\frac{1}{2}}$ in equations (4.16) are now taken as:

$$\widehat{\mathbf{A}}_{j+\frac{1}{2}} = \mathbf{A_\Psi}\left(\mathbf{Q}_i^n, \mathbf{Q}_j^n, \mathbf{n}\right) \ . \tag{4.20}$$

Using algebraic manipulations and equation (4.19), it is easy to prove that the scheme (4.15), (4.17) with (4.20) reduces to the modified *conservative* FORCEα scheme (4.9), (4.11) and (4.12), if $\underline{\underline{\mathbf{A}}}(\mathbf{Q})$ is the Jacobian matrix of a flux $\underline{\underline{\mathbf{F}}}(\mathbf{Q})$.

The choice of the matrices (4.20) has the advantage that the resulting PRICEα-C method becomes exactly conservative if applied to conservation laws. Following the one-dimensional framework, a truly centred approach is now sought. Using

the definition (4.18), the segment path (2.18), and a M-point Gaussian quadrature rule with weights ω_j and positions s_j distributed in the unit interval $[0;1]$, the Roe matrix is approximated numerically as:

$$\mathbf{A}_{\mathbf{\Psi}}(\mathbf{Q}_L, \mathbf{Q}_R, \mathbf{n}) \approx \sum_{j=1}^{M} \omega_j \mathbf{A}(\mathbf{\Psi}(s_j, \mathbf{Q}_L, \mathbf{Q}_R), \mathbf{n}). \tag{4.21}$$

The PRICEα-C scheme, once written in the form (4.15), can be directly compared to the multi-dimensional path-conservative Roe scheme recently proposed by Castro et al. (2008a). It clearly appears that here the matrix $\mathbf{A}_{\mathbf{ij}}^{-}$ does not use explicit wave properties information and it is computed numerically, whereas in Castro et al. (2008a) it is determined as

$$\mathbf{A}_{\mathbf{ij}}^{-} = \mathbf{A}_{\mathbf{\Psi}}^{-}\left(\mathbf{Q}_i^n, \mathbf{Q}_j^n, \mathbf{n}\right) = \mathbf{R}_{\mathbf{\Psi}} \mathbf{\Lambda}_{\mathbf{\Psi}}^{-} \mathbf{R}_{\mathbf{\Psi}}^{-1}, \tag{4.22}$$

where $\mathbf{R}_{\mathbf{\Psi}}$ is the matrix of right eigenvectors of the Roe matrix $\mathbf{A}_{\mathbf{\Psi}}$ and $\mathbf{\Lambda}_{\mathbf{\Psi}}$ is the diagonal matrix with the eigenvalues of $\mathbf{A}_{\mathbf{\Psi}}$. The matrix $\mathbf{\Lambda}_{\mathbf{\Psi}}^{-}$ is, as usual, the negative part of the diagonal matrix $\mathbf{\Lambda}_{\mathbf{\Psi}}$.

In conclusion, also in the multi-dimensional case the proposed formulation avoids the explicit computation of the Roe averages, following the philosophy of centred schemes that, by definition, do not need any wave information on the particular PDE system under consideration.

4.2 High Order Extension

4.2.1 Nonlinear reconstruction technique

In this section the nonlinear reconstruction is described in detail for the two-dimensional case. The procedure, based on the the determination of higher order polynomial reconstructs higher order polynomial data within each spatial cell T_i at time t^n, given the cell averages $\mathbf{Q}_i^n$, allows one to achieve higher spatial and temporal order of accuracy. In particular, the MUSCL procedure has been implemented, that ensures a second order of accuracy in both time and space.

Second order of accuracy, for a two-dimensional framework, is a good compromise between accuracy and complexity of the scheme. The reconstruction procedure relies on the idea of modifying the initial piecewise constant data into piecewise linear functions, where the values at the cell interfaces are thus extrapolated values. For the nonlinear scalar case, the reconstruction operator can be directly applied to the cell averages $\mathbf{Q}_i^n$ of the conserved quantity $\mathbf{Q}$. For nonlinear hyperbolic systems, the reconstruction should be done in characteristic variables (Harten et al., 1987; Dumbser et al., 2007) in order to avoid spurious oscillations that may appear when applying reconstruction operators component-wise to nonlinear hyperbolic systems.

4.2.2 MUSCL-type reconstruction: the two dimensional case.

The extension of second-order accurate schemes to two dimensions involves the construction of an appropriate linear representation of the solution within a computational cell, with a subsequent limiting in order to avoid spurious oscillations in the solution due to the presence of local extrema resulting from the reconstruction process. A number of techniques for reconstructing and limiting the local solution gradients are summarized by Hubbard (1999), who presents a general framework for the construction of slope limiting operators suitable to two-dimensional finite volume schemes on triangular grids. The reconstructed profile considered here is a linear profile, i.e. a plane, leading to a second-order spatial accuracy of the results. The reconstructed profile over the cell i at the time level n, denoted by $\mathbf{w}_i(\mathbf{x}, t^n)$, must in particular satisfy the following constraints:

1. The average value of $\mathbf{w}_i(\mathbf{x}, t^n)$ over the cell i must be equal to the cell average Q_i^n:
$$\frac{1}{|T_i|} \int_{T_i} \mathbf{w}_i(\mathbf{x}, t^n) dx = \mathbf{Q}_i^n, \tag{4.23}$$

2. The value of $\mathbf{w}_i(\mathbf{x}, t^n)$ at the centre $\mathbf{x}_G = (x_G, y_G)$ of the cells j adjacent

to cell i should be as close as possible to the adjacent cell average

$$\mathbf{w}_i(\mathbf{x}_G, t^n) \cong \mathbf{Q}_j^n, \qquad \forall j \in \mathcal{N}_i \tag{4.24}$$

where $\mathcal{N}_i$ denotes the set of cells adjacent to cell i.

Equations (4.23) and (4.24) yield $E_i + 1$ constraints on the function $\mathbf{w}_i(\mathbf{x}, t^n)$, where E_i is the number of neighbours of the cell i . This leads to four conditions for a triangular cell. In most cases, all these conditions cannot be satisfied simultaneously and residual minimisation procedures, such as least-square fitting, must be used to adjust the parameters of the reconstruction. In the following the principles of the two-dimensional linear reconstruction procedure is applied to a scalar variable Q. A similar procedure is applied to a vector variable by considering each component of the vector.

The two-dimensional linear reconstruction $\mathbf{w}_i(\mathbf{x}, t^n)$ of Q in the cell i at the time level n takes the form:

$$\mathbf{w}_i(\mathbf{x}, t^n) = (x - x_i)a_i + (y - y_i)b_i + c_i \tag{4.25}$$

where x_G and y_i are the coordinates of the gravity centre of the ith cell . The reconstructed profile $\mathbf{w}_i(\mathbf{x}, t^n)$ is determined given the average value Q_i^n of Q on the cell i at the time level n and the average values Q_j^n in each of the neighbouring cells.

The reconstructed profile $\mathbf{w}_i(\mathbf{x}, t^n)$ has to satisfy the constraints (4.23) and (4.24). Substituting Equation (4.25) into Equation (4.23) leads to the following condition on c_i:

$$c_i = Q_i^n. \tag{4.26}$$

In order to determine the slopes of the linear profile over the cell, the plane closest to the values Q_j^n is determined by minimizing the square of the distance between the known and reconstructed values, and so minimizing the total residual function

$$R_i(a_i, b_i) = \sum_{j \in \mathcal{N}_i} \left[w_i(\mathbf{x}_G, t^n) - Q_j^n \right]^2. \tag{4.27}$$

The optimal values of a_i and b_i are those for which the derivatives $\partial R_i/a_i$ and $\partial R_i/b_i$ are equal to zero. Substituting Equations (4.25) and (4.26) into Equation (4.27) and differentiating R_i with respect to a_i and b_i yields the following conditions:

$$\sum_{j\in\mathcal{N}_i}(x_j-x_i)^2a_i+(x_j-x_i)(y_j-y_i)b_i+(x_j-x_i)(Q_i^n-Q_j^n)=0 \tag{4.28}$$

$$\sum_{j\in\mathcal{N}_i}(x_j-x_i)(y_j-y_i)a_i+(y_j-y_i)^2b_i+(y_j-y_i)(Q_i^n-Q_j^n)=0 \tag{4.29}$$

that, solved for a_i and b_i, provide:

$$a_i=-\frac{b_i\sum_{j\in\mathcal{N}_i}(x_j-x_i)(y_j-y_i)+\sum_{j\in\mathcal{N}_i}(x_j-x_i)(Q_i^n-Q_j^n)}{\sum_{j\in\mathcal{N}_i}(x_j-x_i)^2}=0 \tag{4.30}$$

$$b_i=\frac{\frac{\sum_{j\in\mathcal{N}_i}(x_j-x_i)(Q_i^n-Q_j^n)\cdot\sum_{j\in\mathcal{N}_i}(x_j-x_i)(y_j-y_i)}{\sum_{j\in\mathcal{N}_i}(x_j-x_i)^2}-\sum_{j\in\mathcal{N}_i}(y_j-y_i)(Q_i^n-Q_j^n)}{\sum_{j\in\mathcal{N}_i}(y_j-y_i)^2-\frac{\left[\sum_{j\in\mathcal{N}_i}(x_j-x_i)(y_j-y_i)\right]^2}{\sum_{j\in\mathcal{N}_i}(x_j-x_i)^2}}=0. \tag{4.31}$$

A slope limiting procedure is now needed in order to ensure that the reconstructed profiles do not induce any undershoots or overshoots of the solution. As suggested by Hubbard (1999), in order to obtain a less restrictive limiter it is chosen to avoid local extrema at the cell-edge midpoint rather than avoiding local extrema at the cell nodes. To this purpose the slopes of the reconstructed profile in the ith cell, they are multiplied by a factor γ, such that

$$0\leq\gamma\leq 1. \tag{4.32}$$

Note the slopes in the x and y directions are reduced by the same factor so that the direction of the slope vector remains unchanged. When applying the limiting procedure to the reconstructed profile U_i^n in the ith cell , at the interface with cell j, the limiter factor γ is calculated as:

$$\gamma=\min_j(\gamma_{i,j}) \qquad \text{with} \qquad j\in\mathcal{N}_i, \tag{4.33}$$

where

$$\gamma_{i,j}=\max[\min(\beta\cdot r_{ij},1),\min(r_{ij},\beta)] \tag{4.34}$$

and

$$r_{ij} = \begin{cases} \Phi\left(\frac{Q_{ij}^{\min} - Q_i^n}{w_i(\mathbf{x}_{ij}, t^n) - Q_i^n}\right) & \text{if} \quad w_i(\mathbf{x}_{ij}, t^n) < Q_i^n \\ \Phi\left(\frac{Q_{ij}^{\max} - Q_i^n}{w_i(\mathbf{x}_{ij}, t^n) - Q_i^n}\right) & \text{if} \quad w_i(\mathbf{x}_{ij}, t^n) > Q_i^n \\ 1 & \text{if} \quad w_i(\mathbf{x}_{ij}, t^n) = Q_i^n \end{cases} \tag{4.35}$$

where $Q_{ij}^{\min} = \min(Q_i, Q_j)$, $Q_{ij}^{max} = \max(Q_i, Q_j)$, while $w_i(\mathbf{x}_{ij}, t^n)$ is the value extrapolated at the interface $\mathbf{x}_{ij} = (x_{ij}, y_{ij})$ from the reconstructed profile w_i. The quantity β in equation (4.34) can take any values between one and two. In particular, $\beta = 1$ and $\beta = 2$ provide, respectively, a two-dimensional version of the one-dimensional Minmod limiter and the Roe's Superbee limiter (see Toro, 1999). Once the reconstruction procedure is carried out for each variable, N non-oscillatory spatial planes $\mathbf{w}_i(\mathbf{x}, t^n)$ are defined at time t^n inside each spatial element T_i and the second order of accuracy is achieved in space.

4.2.3 The fully discrete one-step scheme for the two - dimensional case

The system (4.1) is integrated over a space-time control volume $[T_i] \times [t^n; t^{n+1}]$. The final second-order accurate one-step scheme can be written as follows:

$$\mathbf{Q}_i^{n+1} = \mathbf{Q}_i^n - \frac{1}{|T_i|} \underline{\underline{\mathbf{A}}} \cdot \nabla \mathbf{Q} - \frac{\Delta t}{|T_i|} \sum_{j=1}^{n_f} \mathbf{D}_{j+\frac{1}{2}}^-, \tag{4.36}$$

where

$$\underline{\underline{\mathbf{A}}} \cdot \nabla \mathbf{Q} = \int_{t^n}^{t^{n+1}} \int_{T_i} \underline{\underline{\mathbf{A}}}(\mathbf{Q}_i(\mathbf{x}, t)) \cdot \nabla \mathbf{Q}_i(\mathbf{x}, t) d\mathbf{x} dt \tag{4.37}$$

and

$$\mathbf{D}_{j+\frac{1}{2}}^- = \frac{1}{\Delta t} \int_{t^n}^{t^{n+1}} \int_{S_j} \mathbf{A}_{j+\frac{1}{2}}^- \left(\mathbf{Q}_{jS} - \mathbf{Q}_{iS}\right) dt, \tag{4.38}$$

with

$$\mathbf{Q}_{jS} = \mathbf{Q}_j(\mathbf{x}_{S_j}, t) \qquad , \qquad \mathbf{Q}_{iS} = \mathbf{Q}_i(\mathbf{x}_{S_j}, t), \tag{4.39}$$

and $\mathbf{x}_{S_j}$ the vector that define the edge S_j. All the integrals are approximated using Gaussian quadrature formulae of suitable order of accuracy. Note that the term $\underline{\underline{\mathbf{A}}}(\mathbf{Q}_i(\mathbf{x},t)) \cdot \nabla \mathbf{Q}_i(\mathbf{x},t)$, which integrates the smooth part of the non-conservative product within each cell (excluding the jumps at the boundaries), vanishes for a first order scheme where $\nabla \mathbf{Q}_i(\mathbf{x},t) = 0$. For a second order scheme in space $\nabla \mathbf{Q}_i(\mathbf{x},t) = (a_i, b_i)$, i.e it is constant in (4.37). For a second-order accuracy in time a Gaussian point is necessary for the surface integral (4.38), whereas six Gaussian points are necessary for the volume integral (4.37). The argument of the surface integral in (4.38) is evaluated at the Gaussian point evolving over half a time step the interface-extrapolated vectors by:

$$\mathbf{Q}_{ij}^{n+1/2} = \mathbf{w}_i(\mathbf{x}_{ij}, t^n) - \frac{\Delta t}{2}\left(\mathbf{A}_1(\mathbf{Q}_i^n)\frac{\partial \mathbf{Q}}{\partial x} + \mathbf{A}_2(\mathbf{Q}_i^n)\frac{\partial \mathbf{Q}}{\partial y}\right) \tag{4.40}$$

where the first time derivatives can be directly obtained by a_i and b_i. It is then necessary to evaluate the variable $\mathbf{Q}_i$ in the Gaussian points to calculate the matrices $\underline{\underline{\mathbf{A}}}(\mathbf{Q}_i(\mathbf{x},t))$ appearing into (4.37). Therefore, the local solution $\mathbf{Q}_i(x,t)$ of the PDE in each cell is expanded by a space-time Taylor series with respect to the element barycenter x_G

$$\begin{aligned}
\mathbf{Q}_i(x,t) &= \mathbf{Q}(x_i,t^n) + (x-x_G)\frac{\partial \mathbf{Q}}{\partial x} + (y-y_G)\frac{\partial \mathbf{Q}}{\partial y} + (t-t^n)\frac{\partial \mathbf{Q}}{\partial t}... \\
&= \mathbf{Q}(x_i,t^n) + (x-x_G)\frac{\partial \mathbf{Q}}{\partial x} + (y-y_G)\frac{\partial \mathbf{Q}}{\partial y} + \\
&\quad -(t-t^n)\left(\mathbf{A}_1(Q_i^n)\frac{\partial Q}{\partial x} + \mathbf{A}_2(Q_i^n)\frac{\partial Q}{\partial y}\right)...
\end{aligned} \tag{4.41}$$

Chapter 5

Numerical results for the two-dimensional shallow water equations

In this section the numerical scheme (4.36) is applied to the time-dependent non-linear two-dimensional shallow water equations in the presence of either a fix or a movable bed. Various test cases are considered. In any case the Courant number is set to CFL=0.7 and, as in the one-dimensional case, the matrix (4.21) is evaluated using a three-point Gaussian quadrature rule with the following points s_j and weights ω_j given by (3.1).

5.1 Numerical tests: fix bed

Let us consider the system of shallow water equations with a geometrical source term due to the bottom topography and in absence of bottom friction. The equations are manipulated analytically in order to use the water surface elevation, H, instead of the water depth, h, as conservative variable. In two space dimensions,

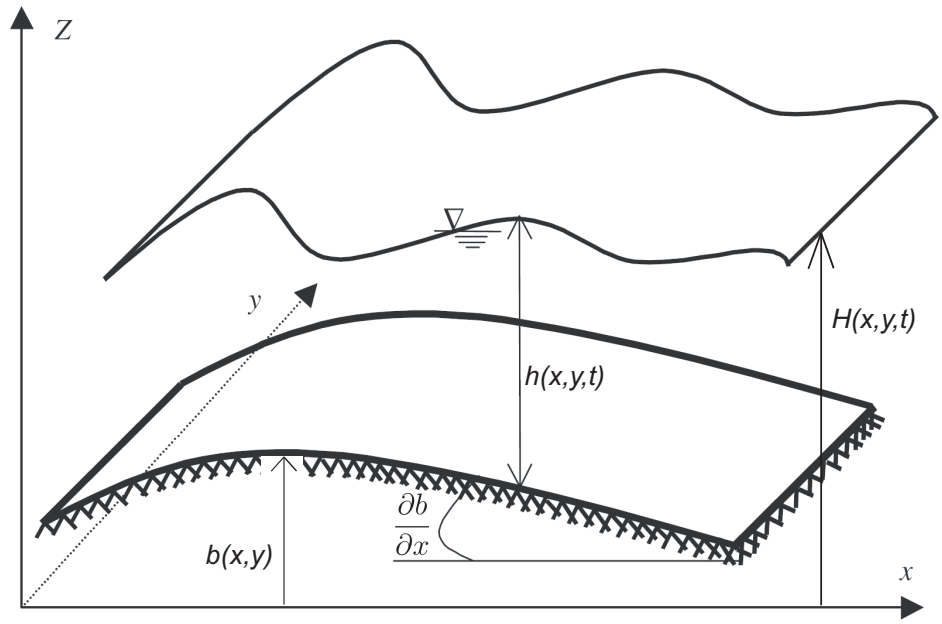

Figure 5.1: Sketch of water surface and channel bottom. Notations are also indicated.

the equations take the form:

$$\begin{cases} \frac{\partial H}{\partial t} + \frac{\partial q_x}{\partial x} + \frac{\partial q_y}{\partial y} = 0 \\ \frac{\partial q_x}{\partial t} + \frac{\partial}{\partial x}\left(\frac{q_x^2}{H-b} + \frac{1}{2}gH^2\right) + \frac{\partial}{\partial y}\left(\frac{q_x q_y}{H-b}\right) + gH\frac{\partial b}{\partial x} = 0 \\ \frac{\partial q_y}{\partial t} + \frac{\partial}{\partial x}\left(\frac{q_y q_x}{H-b}\right) + \frac{\partial}{\partial y}\left(\frac{q_y^2}{H-b} + \frac{1}{2}gH^2\right) + gH\frac{\partial b}{\partial y} = 0\ , \end{cases} \tag{5.1}$$

where $H(x, y, t)$ denotes the water surface elevation, $q(x, y, t)$ is the discharge for unit width, $b(x, y)$ represents the given bed topography (Fig. 5.1). $\partial b/\partial x$ and $\partial b/\partial y$ are the bed slopes in the x and y direction respectively. System (5.1), together with the trivial equation $\frac{db}{dt} = 0$, can be written in the nonconservative form (4.1), with the vector $\mathbf{Q}$ and matrix $\mathbf{A}_1$ and $\mathbf{A}_2$ given by:

$$\mathbf{Q} = \begin{bmatrix} H \\ q_x \\ q_y \\ b \end{bmatrix} \quad , \quad \mathbf{A}_1 = \begin{bmatrix} 0 & 1 & 0 & 0 \\ g(H-b) - \frac{q_x^2}{(H-b)^2} & \frac{2q_x}{H-b} & 0 & \frac{q_x^2}{(H-b)^2} \\ -\frac{q_x q_y}{(H-b)^2} & \frac{q_y}{H-b} & 0 & \frac{q_x q_y}{(H-b)^2} \\ 0 & 0 & 0 & 0 \end{bmatrix},$$

$$\mathbf{A}_2 = \begin{bmatrix} 0 & 0 & 1 & 0 \\ -\frac{q_x q_y}{(H-b)^2} & \frac{q_y}{H-b} & 0 & \frac{q_x q_y}{(H-b)^2} \\ g(H-b) - \frac{q_y^2}{(H-b)^2} & 0 & \frac{2q_y}{H-b} & \frac{q_y^2}{(H-b)^2} \\ 0 & 0 & 0 & 0 \end{bmatrix}. \qquad (5.2)$$

In the following, we consider different case test, selected in order to verify a specific property of the numerical scheme. In particular, a cicular dam-break problem is considered to check the ability of the method to preserve symmetry. Another test is used to check the behaviour of the scheme in the case of a small perturbation of a quiescent state. Finally, a movable bed test is considered in which the propagation of a two-dimensional bump is analyzed.

5.1.1 Circular dam-break problem

This example consists of the instantaneous breaking of a cylindrical tank (diameter 20 m) initially filled with 2 m of water at rest. The wave generated by the breaking of the tank propagates into still water with an initial depth of 0.5 m. Figure 5.2 illustrates this wave propagation on a computational mesh of 9724 elements using the proposed PRICE2-C scheme (4.36). When the column of water is released, the shock wave results in a dramatic increase of water depth in the lower depth region propagating in the radial direction. The test can be useful to check the ability of the method to preserve cylindrical symmetry. Indeed, the problem becomes 1D in the radial direction and a theoretical solution can be obtained. This solution, expressed in a radial coordinate system, reads (LeVeque, 2002):

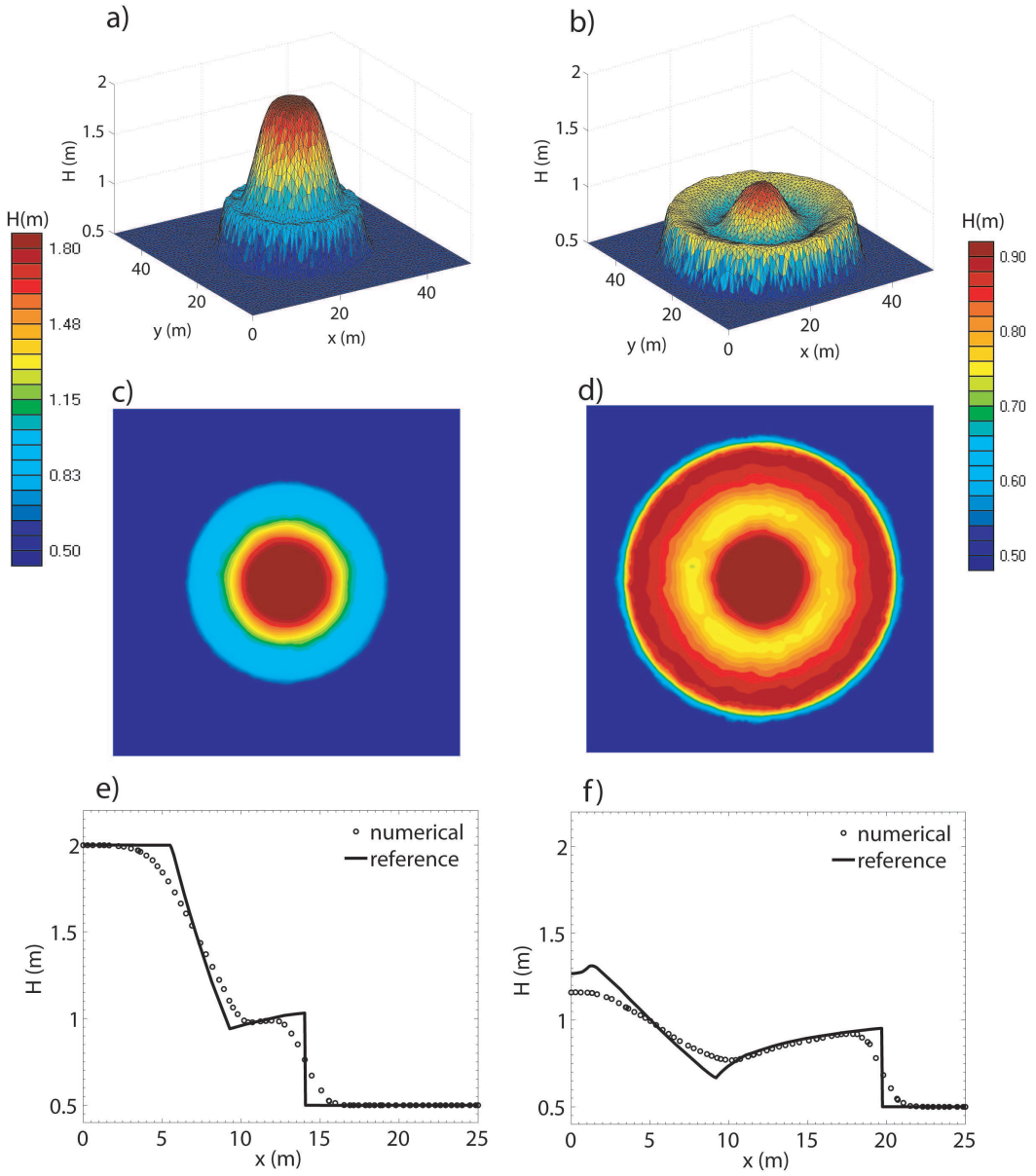

Figure 5.2: Numerical results of the PRICE2-C scheme (4.36) for the circular dam-break test at t=1 s (left column), and at t=2.5 s (right column). Figure a,b show the tridimensional view of the water surface elevation. Figure c,d show the plan view of the same surface. and Figure e,f show the comparison between the two-dimensional numerical solution along a radial direction (symbols) and the pseudo-analytical solution (line).

$$\begin{cases} \frac{\partial H}{\partial t} + \frac{\partial q_r}{\partial x} = -\frac{q_r}{r} \\ \frac{\partial q_r}{\partial t} + \frac{\partial}{\partial x}\left(\frac{q_r^2}{H} + \frac{1}{2}gH^2\right) = -\frac{q_r^2}{rH} \ , \end{cases} \tag{5.3}$$

where r is the radius and $q_r = Hv_r$, v_r being the radial velocity. Equations (5.3), solved by the monodimensional PRICE-C scheme introduced in chapter 2, provide a pseudo-analytical solution to be compared with the numerical solution.

Figures 5.2a,b show a three dimensional view of the dam break after 1 s and 2.5 s, while figures 5.2c,d show the corresponding planar view. It clearly appears the outward-propagating circular shock and wave and the inward-propagating circular rarefaction wave. The figures confirm that the method is able to preserve the cylindrical symmetry, and demonstrate the effectiveness of an unstructured triangular mesh to represent this problem. Finally figure 5.2e,f show the sectional view (a cut along a given radial direction) of the 2D dam break. There is a good agreement between the numerical solution and the pseudo-analytical solution, and spurious oscillations are absent

5.1.2 Small perturbation of a two dimensional steady state water

This test case is the two-dimensional analogous of the test case dicussed in chapter 3.1.2, and it was first proposed by LeVeque (1998). The equations are solved in a rectangular domain $[0, 2] \times [0, 1]$. The two-dimensional bottom topography consists in an elliptical bump:

$$b(x, y) = 0.8e^{(-5(x-0.9)^2-50(y-0.5)^2)} \ . \tag{5.4}$$

Moreover, the initial water surface and discharge are given by :

$$\begin{aligned} H(x, y, 0) &= \begin{cases} 1+\epsilon & \text{if} \quad 0.05 \leq x \leq 0.15 \text{ m} \\ 1 & \text{otherwise} \end{cases} \\ q_x(x, y, 0) &= 0 \\ q_y(x, y, 0) &= 0 \end{aligned} \tag{5.5}$$

The surface is flat everywhere except for $0.05 \leq x \leq 0.15$ m, where a perturba-

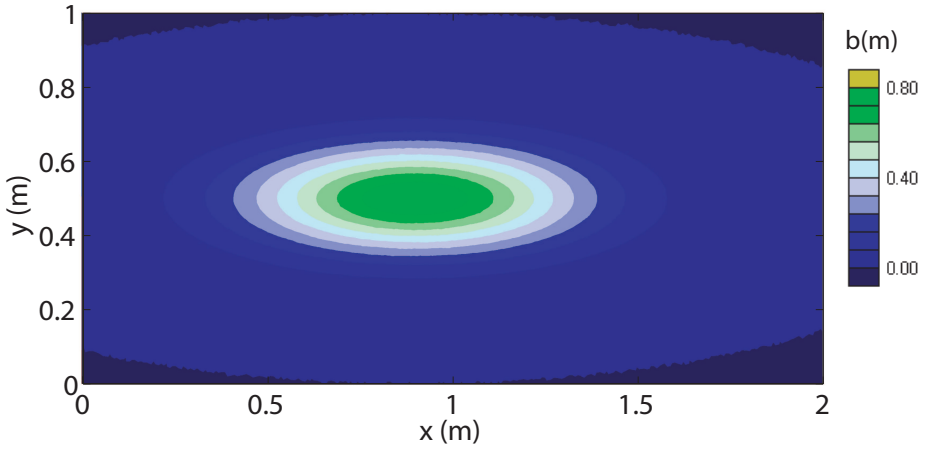

Figure 5.3: Elliptical initial condition for the bed elevation as given by eq. (5.4).

tion ($\epsilon = 0.01$ m) is provided. Transmissive boundary conditions are prescribed on the right side and on the left side of the rectangular domain, whereas reflective conditions are prescribed on the upper and lower sides. The initial conditions and the elliptical bump are depicted in Fig. 5.3. Fig. 5.4 shows the results obtained with a computational mesh of 52692 cells. Due to the transmissive boundary conditions, the left propagating pulse has already left the domain at the first time shown, hence Fig. 5.4 shows only the right-going portion of the disturbance as it propagates over the hump. Note that the wave speed is slower above the hump than elsewhere, thus implying a distortion of the initially planar perturbation. No spurious oscillations are present and there is a good agreement with the numerical results given by LeVeque (1998).

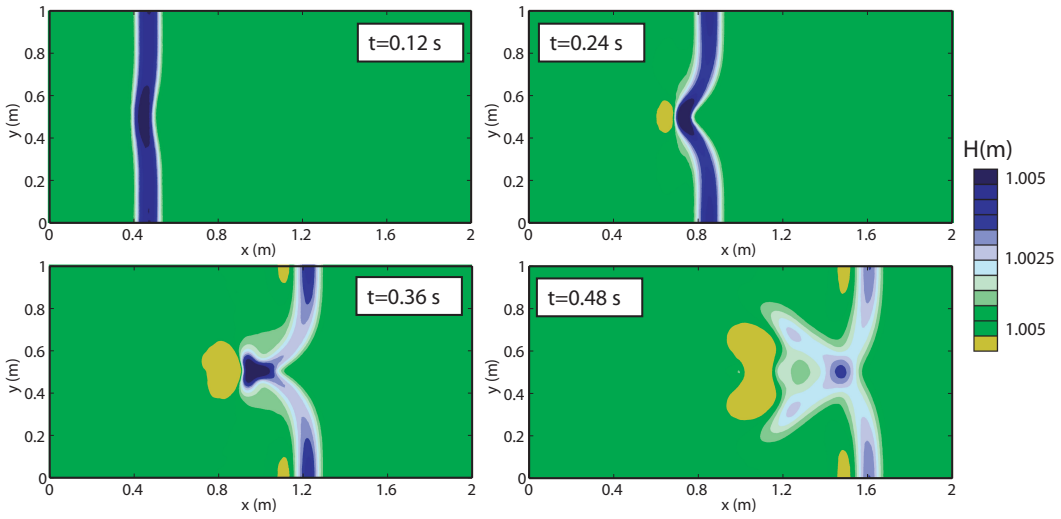

Figure 5.4: Numerical results of the PRICE2-C scheme (4.36) for a small perturbation of a two dimensional steady state water travelling over a bump. Planar views of the water surface at $t = 0.12$, $t = 0.24$, $t = 0.36$ and $t = 0.48$ s are shown. and the exact solution (line).

5.2 Movable bed test

We now consider shallow water equations (5.1) coupled with the two-dimensional Exner equation:

$$\frac{\partial b}{\partial t} + \frac{\partial q_{sx}}{\partial x} + \frac{\partial q_{sy}}{\partial y} = 0, \tag{5.6}$$

where $b = b(x, y, t)$ is now the time-varying bottom elevation and (q_{sx}, q_{sy}) are the intensities of bed-load rate per unit width in the x and y directions respectively. These latter quantities read:

$$(q_{sx}, q_{sy}) = \mathbf{q}_s \cdot (\cos\alpha, \sin\alpha) \tag{5.7}$$

where α is the angle denoting the direction of sediment transport with rispect of the x axis computed according to an anticlockwise direction) while $\mathbf{q}_s$ is the absolute volue of bed-load rate per unit width. It then results that sinα and

cosα are:

$$\sin\alpha = \frac{q_y}{\sqrt{(q_x^2+q_y^2)}}$$
$$\cos\alpha = \frac{q_x}{\sqrt{(q_x^2+q_y^2)}} \tag{5.8}$$

Setting $q = \sqrt{(q_x^2+q_y^2)}$, we can compute $\mathbf{q}_s$ by any of the one-dimensional relations (3.19), (3.21), (3.16). Similarly to the one-dimensional case the porosity term is incorporated in q_s.

The system of governing equations describing the coupled evolution of the fluid and the bed can be written in the form (4.1) with vector $\mathbf{Q}$ and matrix $\mathbf{A}_1$ and $\mathbf{A}_2$ being respectively:

$$\mathbf{Q} = \begin{bmatrix} H \\ q_x \\ q_y \\ b \end{bmatrix}, \quad \mathbf{A}_1 = \begin{bmatrix} \frac{\partial q_{sx}}{\partial H} & 1+\frac{\partial q_{sx}}{\partial q_x} & \frac{\partial q_{sx}}{\partial q_y} & \frac{\partial q_{sx}}{\partial b} \\ g(H-b)-\frac{q_x^2}{(H-b)^2} & \frac{2q_x}{H-b} & 0 & \frac{q_x^2}{(H-b)^2} \\ -\frac{q_xq_y}{(H-b)^2} & \frac{q_y}{H-b} & 0 & \frac{q_xq_y}{(H-b)^2} \\ \frac{\partial q_{sx}}{\partial H} & \frac{\partial q_{sx}}{\partial q_x} & \frac{\partial q_{sx}}{\partial q_y} & \frac{\partial q_{sx}}{\partial b} \end{bmatrix},$$

$$\mathbf{A}_2 = \begin{bmatrix} \frac{\partial q_{sy}}{\partial H} & \frac{\partial q_{sy}}{\partial q_x} & 1+\frac{\partial q_{sy}}{\partial q_y} & \frac{\partial q_{sy}}{\partial b} \\ -\frac{q_xq_y}{(H-b)^2} & \frac{q_y}{H-b} & 0 & \frac{q_xq_y}{(H-b)^2} \\ g(H-b)-\frac{q_y^2}{(H-b)^2} & 0 & \frac{2q_y}{H-b} & \frac{q_y^2}{(H-b)^2} \\ \frac{\partial q_{sy}}{\partial H} & \frac{\partial q_{sy}}{\partial q_x} & \frac{\partial q_{sy}}{\partial q_y} & \frac{\partial q_{sy}}{\partial b} \end{bmatrix}. \tag{5.9}$$

where the derivatives of q_{sx} and q_{sy} with respect to the unknown variables are shown. Note that the continuity equation of the fluid has been suitably changed to take into account the variability of bed elevation. In the following the results provided by the PRICE2-C scheme are presented.

5.2.1 Evolution of a bottom hump

For purposes of verifying our finite volume scheme, a simplified test example is here used. It consists in the evolution of an initial hump in a squared channel.

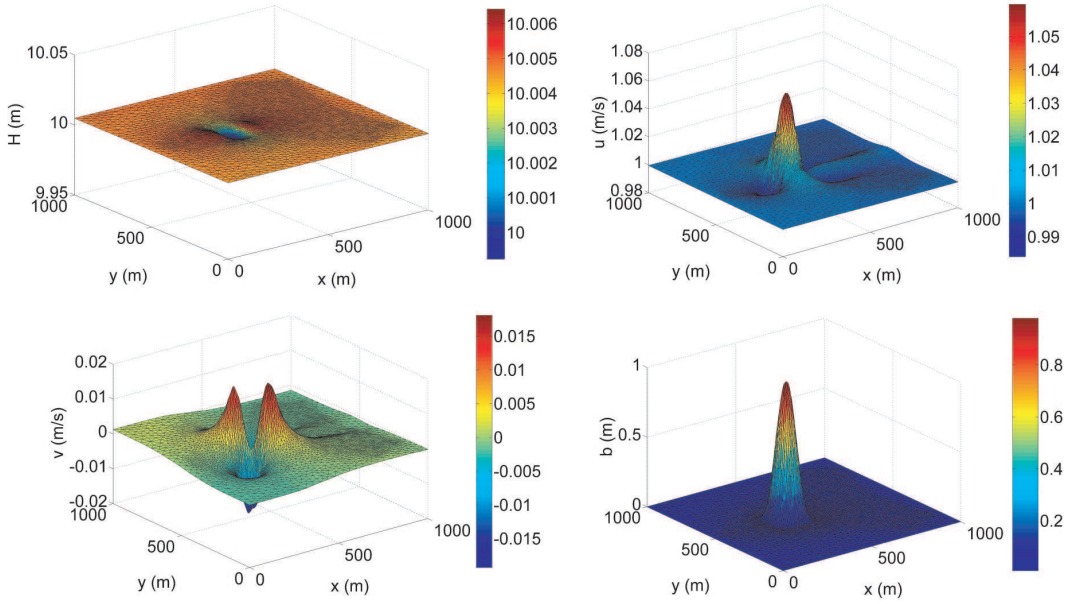

Figure 5.5: Numerical results of the PRICE2-C scheme (4.36) for a steady flow over a bump. Equilibrium condition for the water surface H and the velocities u and v (respectively along x and along y) for the fixed bed case is shown. The bed elevation is also shown. These results will be the initial conditions for the movable bed simulation.

This test case was first introduced by Hudson and Sweby (2005). The initial hydrodynamic condition are given by:

$$H(x,y,0) = 10\,\mathrm{m} \quad , \quad q_x = (x,y,0) = 10\,\mathrm{m}^2/\mathrm{s} \quad , \quad q_y = (x,y,0) = 0. \tag{5.10}$$

The initial hump is given by:

$$b(x) = \begin{cases} \sin^2\left(\frac{\pi(x-300)}{200}\right)\sin^2\left(\frac{\pi(y-400)}{200}\right) & \text{if } 300 \le x \le 500\text{m}\ ,\ 400 \le y \le 600\text{m} \\ 0 & \text{otherwise}\ . \end{cases} \tag{5.11}$$

A constant discharge $q_x = 10\mathrm{m}^2/\mathrm{s}$ is prescribed in time at the upstream boundary and at all the other boundaries transmissive conditions are assumed. The model is first run toward the equilibrium state, keeping the river bed fixed. In

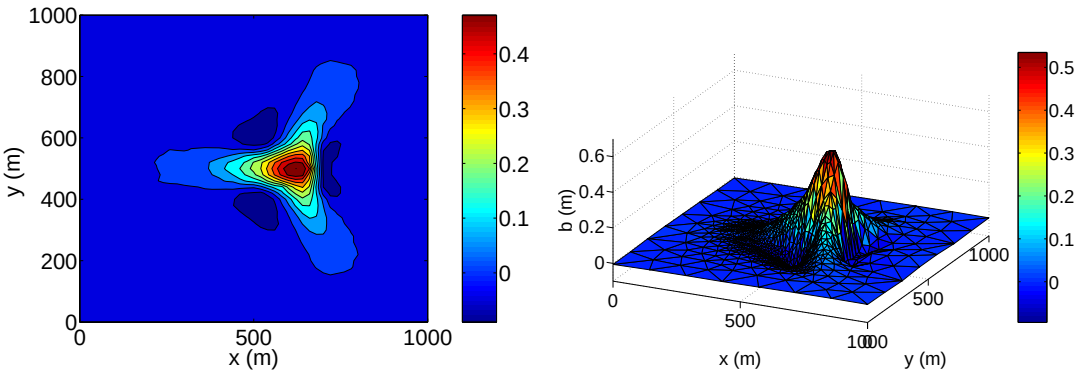

Figure 5.6: Numerical results of the PRICE2-C scheme (4.36) for the evolution of a bottom hump with A=0.001. Planar view (left) and three dimensional view (right) of the bottom elevation after 100 h.

order to obtain this equilibrium solution, the time integration process is stopped when the inequality

$$\frac{\|Q^{n+1} - Q^n\|}{\|Q^n\|} < \tau \tag{5.12}$$

is satisfied. Here $\|\cdot\|$ denotes the L_1-norm and τ is a given tolerance fixed to 10^{-7} in the computation. The equilibrium state is shown in Fig. (5.5) and follows very closely the results presented by Hudson and Sweby (2005) by means of an upwind method. The capability of the present centred method to reach an equilibrium state confirms that the bed-slope term is correctly balanced with the fluxes (well-balanced scheme).

Now a movable bed is considered and bed-load is computed by the Grass power-law formula (3.16). The parameter A is fixed equal to 0.001, so modelling a weak interaction between water and sediments (Hudson and Sweby, 2005). The value $m = 3$ and $\lambda_p = 0.4$ are also chosen. For this kind of problem the initial topography of the river bed gradually changes into a star-shaped pattern, which spreads out over in time. De Vriend (1987) derived an approximate solution for the angle of spread of this pattern when A <0.2. The analytical approximation

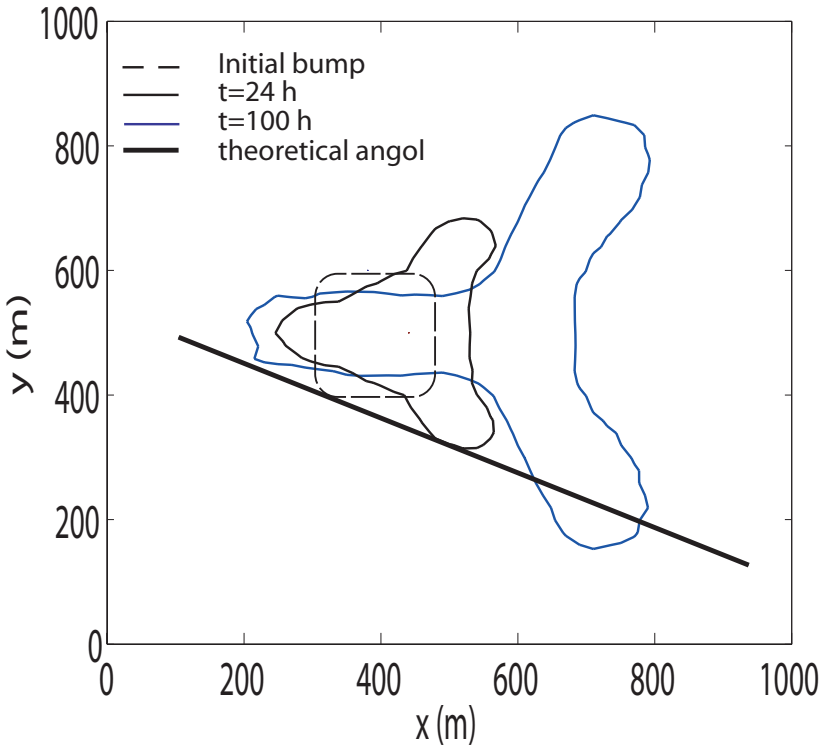

Figure 5.7: The angle of spread of the star shaped bottom pattern. The theoretical angle of spreading given by 5.14 is also shown

of this angle of spread θ is given by (see De Vriend, 1987):

$$\tan\theta = 3\sqrt{3}\frac{(m-1)}{9m-1} \tag{5.13}$$

and with $m = 3$ it reads:

$$\theta = \tan^{-1}\frac{3\sqrt{3}}{13} = 21.787^{\circ}. \tag{5.14}$$

Results after $t = 100$h are presented in Fig. 5.6. The scheme produces smooth results that do not suffer from spurious oscillations. The star-shaped pattern is also reproduced. Fig.(5.7) shows the comparison between different bed level curves (b=0.05 cm), at three different times, and the theoretical approximation of the angle of spread, θ, as given by (5.14). There is a good agreement between the numerical and analytical solutions. The comparison with similar numerical

results available in literature (see Hudson and Sweby, 2005; Delis and Papoglou, 2008) and provided by upwind-type schemes is also satisfactory. This demonstrate the ability of the present high order scheme to predict long term movement of bed perturbations, in spite of the scheme does not include any information about the directions of propagation of the disturbances.

Chapter 6

Conclusions

This thesis is centred on the development of a simple numerical tool to solve the coupled De Saint Venant-Exner system. From a mathematical point a view this system of equations is hyperbolic. It means that the solution admits both discontinuous and smooth solutions. Even for the case in which the initial conditions are smooth, the non-linear character combined with the hyperbolic type of the equations can lead to discontinuous solutions in a finite time. Aware of this aspect, the attention was directed toward the numerical modelling of river hydrodynamics and morphodynamics with particular attention to physical phenomena in which water surface discontinuities and sediment fronts are present. To correctly capture discontinuous solutions, different numerical techniques have been developed in the last decades. In particular, the finite volume method had undergone a great increase of popularity since it easily deals with discontinuities of the solution and it conserves the variables on a coarse mesh, an important requirement especially for fluid dynamic problems. Shallow water type models contain the bed slope term, usually treated as a source term, since it is a non-conservative term that can not be recast in conservative form. It is well known since the work of Bermudez and Vazquez (1994) that the presence of the bed slope term in a finite volume framework can affect the quality of the results especially

when steady or nearly steady state solutions are approached. In this case only sophisticated schemes can perform adequately. When solving real problems one is likely to encounter all sorts of situations, with a high probability that naive schemes will compromise the quality and reliability of the solution. To handle such problems, the concept of well-balanced schemes, that is, schemes that preserves all equilibria of the system or a family of them, has been considered by several authors. The present scheme is shown to correctly solve balances between sources and fluxes when applied to a great variety of steady and unsteady test cases. This is extremely important in the movable-bed case, because the well-balancing of the scheme allows to reproduce small perturbations of the free surface and of the bottom elevation, otherwise of the same order of magnitude of the numerical errors induced by the non-balancing.

The scheme is also shown to be shock-capturing, since it correctly estimates both the front strength and speed of propagation. Moreover in the presence of discontinuous solutions the numerical method produces essentially non-oscillatory numerical results.

The scheme is extended to high order of accuracy in space and time via the ADER-WENO and MUSCL technique respectively for the one- and two-dimensional case. The achievement of higher-order accuracy allows us to use coarse grids thereby increasing the computational efficiency of the scheme. This goal is desirable when natural morphodynamics phenomena, characterized by long time scales, must be studied.

Moreover note that this work represents the first attempt to solve a non-conservative system using the theory of Dal Maso et al. (1995) by a centred approach. The theoretical derivation of the scheme is kept general throughout the thesis, hence a framework for constructing high-order numerical centred schemes is proposed and it can be applied to any hyperbolic system containing non-conservative terms. Hence the strength of the present method consists of a large applicability in a broad range of engineering problems, since no mention is done to the eigenstructure of the hyperbolic system of equations. For example, the scheme can be applied to the two-layer shallow water equations for solving

stratified flows and Savage−Huter type models (Savage and Hutter, 1991) for solving avalanches of granular materials. Testing the behaviour of the proposed scheme for these systems of equations will be the subject of future research.

Bibliography

P. Arminjon and A. St-Cyr. Nessyahu-Tadmor-type central finite volume methods without predictor for 3D Cartesian and unstructured tetrahedral grids. *Applied Numerical Mathematics*, 46(2):135–155, AUG 2003. ISSN 0168-9274. doi: 10.1016/S0168-9274(03)00025-4.

P. Arminjon and M.C. Viallon. Convergence of a finite volume extension of the Nessyahu-Tadmor scheme on unstructured grids for a two-dimensional linear hyperbolic equation. *Siam Journal on Numerical Analysis*, 36(3):738–771, APR 29 1999. ISSN 0036-1429.

P. Arminjon, M.C. Viallon, and A. Madrane. A finite volume extension of the Lax-Friedrichs and Nessyahn-Tadmor schemes for conservation laws on unstructured grids. *International Journal of Computational Fluid Dynamics*, 9 (1):1–22, 1997. ISSN 1061-8562.

M.B. Bellal, C. Spinewine, and Y. Zech. Morphological evolution of steep-sloped river beds in the presence of a hydraulic jump. In *Experimental study, paper presented at XXX IAHR congress*, pages 133–140, 2003.

A Bermudez and E Vazquez. Upwind methods for hyperbolic conservation-laws with source terms. *Computers & Fluids*, 23(8):1049–1071, NOV 1994. ISSN 0045-7930.

F Bianco, G Puppo, and G Russo. High-order central schemes for hyperbolic systems of conservation laws. *Siam Journal on Scientific Computing*, 21(1): 294–322, SEP 22 1999. ISSN 1064-8275.

S Bryson and D Levy. Balanced central schemes for the shallow water equations on unstructured grids. *Siam Journal on Scientific Computing*, 27(2):532–552, 2005. ISSN 1064-8275. doi: 10.1137/040605539.

V. Caleffi, A. Valiani, and Bernini B. High-order balanced cweno scheme for movable bed shallow water equations. *Advances in Water Resources*, 30:730–741, 2007.

V. Caleffi, A. Valiani, and A. Bernini. Fourth-order balanced source term treatment in central WENO schemes for shallow water equations. *Journal of Computational Physics*, 218(1):228–245, OCT 10 2006. ISSN 0021-9991. doi: 10.1016/j.jcp.2006.02.001.

Z. Cao, R. Day, and A. Egashira. Coupled and decoupled numerical modeling of flow and morphological evolution in alluvial rivers. *Journal of Hydraulic Engineerings, ASCE*, 128(3):306–321, 2002.

Z Cao, G Pender, S Wallis, and P Carling. Computational dam-break hydraulics over erodible sediment bed. *Journal of Hydraulic Engineering-Asce*, 130(7):689–703, JUL 2004. ISSN 0733-9429. doi: 10.1061/(ASCE)0733-9429(2004)130:7(689).

M. Castro, E. Fernández-Nieto, A. Ferreiro, J. García-Rodríguez, and C. Parés. High order extensions of roe schemes for two-dimensional nonconservative hyperbolic systems. *Journal of Scientific Computing*, 2008a. doi: http://dx.doi.org/10.1007/s10915-008-9250-4.

M. Castro, E. D. Ferndandez-Nieto, and A.M. Ferreiro. Sediment transport models in Shallow Water equations and numerical approach by high order finite volume methods. *Computers & Fluids*, 37(3):299–316, MAR 2008b. ISSN 0045-7930. doi: 10.1016/j.compfluid.2007.07.017.

M.J. Castro, J.M. Gallardo, and C. Parés. High-order finite volume schemes based on reconstruction of states for solving hyperbolic systems with non-

conservative products. applications to shallow-water systems. *Mathematics of Computations*, 75:1103–?1134, 2006.

L. Correia, B. Krishnappan, and W. Graf. Fully coupled unsteady mobile boundary flow model. *Journal of Hydraulic Engineering, ASCE*, 118(3):476–494, 1992.

R. Courant, E. Isaacson, and M. Rees. On the solution of nonlinear hyperbolic differential equations by finite differences. *Comm. Pure Appl. Math. Vol.*, 118: 243–255, 1952.

N. Crnjaric-Zic, S. Vukovic, and L. Sopta. Extension of eno and weno schemes to one-dimensional bed-load sediment transport equations. *Computers & Fluids*, 33(1):31–56, 2003.

N Crnjaric-Zic, S Vukovic, and L Sopta. Balanced finite volume WENO and central WENO schemes for the shallow water and the open-channel flow equations. *Journal of Computational Physics*, 200(2):512–548, NOV 1 2004. ISSN 0021-9991. doi: 10.1016/j.jcp.2004.04.012.

J. Cunge, A. Verwey, and F. M. Holly. *Practical aspects of computational river hydraulics.* Pitman Advanced Publishing Program, London., 1980.

J.A. Cunge and N. Perdreau. La houille blanche. *Journal de Mathematiques pures et appliquées*, 7:561–570, 1973.

G Dal Maso, PG LeFloch, and F Murat. Definition and weak stability of nonconservative products. *Journal de Mathematiques pures et appliquées*, 74(6): 483–548, 1995. ISSN 0021-7824.

H.J. De Vriend. 2dh mathematical modelling of morphological evolutions in shallow water. *Coastal Eng.*, 11:1–27, 1987.

A Defina. Numerical experiments on bar growth. *Water Resources Research*, 39 (4), APR 11 2003. ISSN 0043-1397. doi: 10.1029/2002WR001455.

A.I. Delis and I. Papoglou. Relaxation approximation to bed-load sediment transport. *Journal of Computational and Applied Mathematics*, 213:521–546, 2008.

M. Dumbser and M. Käser. Arbitrary high order non-oscillatory finite volume schemes on unstructured meshes for linear hyperbolic systems. *Journal of Computational Physics*, 221:693–723, 2007.

M. Dumbser and C.D. Munz. Building blocks for arbitrary high order discontinuous Galerkin schemes. *Journal of Scientific Computing*, 27:215–230, 2006.

M. Dumbser, M. Käser, V.A Titarev, and E.F. Toro. Quadrature-free non-oscillatory finite volume schemes on unstructured meshes for nonlinear hyperbolic systems. *Journal of Computational Physics*, 226:204–243, 2007.

M. Dumbser, D. Balsara, E.F. Toro, and C.D. Munz. A unified framework for the construction of one-step finite-volume and discontinuous Galerkin schemes. *Journal of Computational Physics*, 227:8209–8253, 2008a.

M. Dumbser, C. Enaux, and E.F. Toro. Finite volume schemes of very high order of accuracy for stiff hyperbolic balance laws. *Journal of Computational Physics*, 227:3971–4001, 2008b.

J. M. Gallardo, C. Pares, and M. Castro. On a well-balanced high-order finite volume scheme for shallow water equations with topography and dry areas. *Journal of Computational Physics*, 227(1):574–601, NOV 10 2007. ISSN 0021-9991. doi: 10.1016/j.jcp.2007.08.007.

P Garcia-Navarro and ME Vazquez-Cendon. On numerical treatment of the source terms in the shallow water equations. *Computers & Fluids*, 29(8):951–979, NOV 2000. ISSN 0045-7930.

J Glimm. Solution in the large for nonlinear hyperbolic systems of equations. *Communications on Pure and Applied Mathematics*, 18:697–715, 1965.

S.K. Godunov. A difference scheme for numerical computation of discontinuous solution of hydrodynamic equations. *Mathematics of the USSR-Sbornik*, M 43: 271–306, 1959.

L. Gosse. A well-balanced flux-vector splitting scheme designed for hyperbolic systems of conservation laws with source terms. *Computers & Mathematics with Applications*, 39(9-10):135–159, MAY 2000. ISSN 0898-1221.

N. Goutal and F. Maurel. Proceedings of the second workshop on dam-breakwave simulation. Technical Report HE-43/97/016/A, Electricité de France, Département Laboratoire National d'Hydraulique, Groupe Hydraulique Fluviale, 1997.

H. Graf and M. S. Altinakar. Fluvial hydraulics. flow and transport processes in channels of simple geometry. Chichester, Wiley, 1998.

A.J. Grass. Sediments transport by waves and currents. *SERC London Cent Mar Technol, Report No. FL29;*, 1981.

A. Harten, B. Engquist, S. Osher, and S. Chakravarthy. Uniformly high order essentially non-oscillatory schemes, III. *Journal of Computational Physics*, 71: 231–303, 1987.

F. Holly and J. Rahuel. New numerical/physical framework for mobile bed modelling, part 1: Numerical and physical principles. *Journal of Hydraulic Research*, 28(4):401–416, 1990.

T.Y. Hou and P LeFloch. Why Non–Conservative Schemes Converge to the Wrong Solutions: Error Analysis. *Math. of Comput.*, 62:497–530, 1994.

M.E. Hubbard. Multidimensional slope limiters for muscl-type finite volume schemes on unstructured grids. *Journal of Computational Physics*, 155:54–74(21), 1999.

ME Hubbard and P Garcia-Navarro. Flux difference splitting and the balancing of source terms and flux gradients. *Journal of Computational Physics*, 165(1): 89–125, NOV 20 2000. ISSN 0021-9991.

J. Hudson and P.K. Sweby. A high-resolution scheme for the equations governing 2d bed-load sediment transport. *International Journal for Numerical Methods in Fluids*, 47:1085–1091, 2005.

G.S. Jiang and C.W. Shu. Efficient implementation of weighted ENO schemes. *Journal of Computational Physics*, 126:202–228, 1996.

GS Jiang and E Tadmor. Nonoscillatory central schemes for multidimensional hyperbolic conservation laws. *SIAM Journal on Scientific Computing*, 19(6): 1892–1917, NOV 1998. ISSN 1064-8275.

GS Jiang, D Levy, CT Lin, S Osher, and E Tadmor. High-resolution nonoscillatory central schemes with nonstaggered grids for hyperbolic conservation laws. *SIAM Journal on Numerical Analysis*, 35(6):2147–2168, NOV 16 1998. ISSN 0036-1429.

A. Kassem and M. Chaudry. Comparison of coupled and semicoupled numerical models for alluvial channels. *Journal of Hydraulic Engineering,ASCE*, 124(8): 794–802, 1998.

B. Krishnappan. Modelling of unsteady flows in alluvial streams. *Journal of Hydraulic Engineering,ASCE*, 111(2):257–266, 1985.

A Kurganov and G Petrova. Central-upwind schemes on triangular grids for hyperbolic systems of conservation laws. *Numerical Methods for Partial Differential Equations*, 21(3):536–552, MAY 2005. ISSN 0749-159X. doi: 10.1002/num.20049.

A. Kurganov and G. Petrova. A second-order well-balanced positivity preserving central-upwind scheme for the Saint-Venant system. *Communications in Mathematical Sciences*, 5(1):133–160, MAR 2007. ISSN 1539-6746.

A Kurganov and E Tadmor. New high-resolution central schemes for nonlinear conservation laws and convection-diffusion equations. *Journal of Computational Physics*, 160(1):241–282, MAY 1 2000. ISSN 0021-9991.

M Kuther. Error estimates for the staggered Lax-Friedrichs scheme on unstructured grids. *SIAM Journal on Numerical Analysis*, 39(4):1269–1301, DEC 4 2001. ISSN 0036-1429.

C.T. Lai. Modeling alluvial-channel flow by multimode characteristics method. *Journal of Engineering Mechanics-ASCE*, 117(1):32–53, JAN 1991. ISSN 0733-9399.

S. Lanzoni, A. Siviglia, A. Frascati, and G. Seminara. Long waves in erodible channels and morphodynamic influence. *Water Resour. Res.*, 42:257–266, 2006. doi: 10.1029/ 2006WR004916.

P.D. Lax. Weak solutions of nonlinear hyperbolic equations and their numerical computations. *Communications of Pure and Applied Mathematics*, 44:21–41, 1954.

RJ LeVeque. Balancing source terms and flux gradients in high-resolution Godunov methods: The quasi-steady wave-propagation algorithm. *Journal Of Computational Physics*, 146(1):346–365, OCT 10 1998. ISSN 0021-9991.

RJ LeVeque. *Finite Volume Methods For Hyperbolic Problems.* Cambridge University Press,, 2002.

D Levy, G Puppo, and G Russo. Central WENO schemes for hyperbolic systems of conservation laws. *ESAIM-Mathematical Modelling and Numerical Analysis*, 33(3):547–571, MAY-JUN 1999. ISSN 0764-583X.

D Levy, G Puppo, and G Russo. A fourth-order central WENO scheme for multidimensional hyperbolic systems of conservation laws. *SIAM Journal on Scientific Computing*, 24(2):480–506, OCT 31 2002. ISSN 1064-8275.

S. Li. High order central scheme on overlapping cells for magneto-hydrodynamic flows with and without constrained transport method. *Journal of Computational Physics*, 227(15):7368–7393, JUL 20 2008. ISSN 0021-9991. doi: 10.1016/j.jcp.2008.04.022.

XD Liu and E Tadmor. Third order nonoscillatory central scheme for hyperbolic conservation laws. *Numerische Mathematik*, 79(3):397–425, MAY 1998.

X.D. Liu, S. Osher, and T. Chan. Weighted essentially non-oscillatory schemes. *Journal of Computational Physics*, 115:200–212, 1994.

Y. Liu, C.W. Shu, E. Tadmor, and M. Zhang. Non-oscillatory hierarchical reconstruction for central and finite volume schemes. *Communications in Computational Physics*, 2(5):933–963, OCT 2007. ISSN 1815-2406.

YJ Liu. Central schemes on overlapping cells. *Journal of Computational Physics*, 209(1):82–104, OCT 10 2005. ISSN 0021-9991. doi: 10.1016/j.jcp.2005.03.014.

D. Lyn. Unsteady sediment transport modeling. journal of hydraulic engineering. *Journal of Hydraulic Engineering, ASCE*, 113(1):1–15, 1987.

D.A. Lyn and M. Altinakar. St. Venant Exner equations for near-critical and transcritical flows. *Journal of Hydraulic Engineering, ASCE*, 128(6):579–587, 2002.

EA Meselhe and FM Holly. Invalidity of Preissmann scheme for transcritical flow. *Journal of Hydraulic Engineering-ASCE*, 123(7):652–655, JUL 1997. ISSN 0733-9429.

Meyer-Peter and Müller. Formulas for bed-load transport. In *Report on 2nd meeting on international association on hydraulic structures research*, pages 39–64. Stockholm, 1948.

H Nessyahu and E Tadmor. Non-oscillatory central differencing for hyperbolic conservation-laws. *Journal of Computational Physics*, 87(2):408–463, APR 1990. ISSN 0021-9991.

S Noelle, W Rosenbaum, and M Rumpf. 3D adaptive central schemes: Part I. Algorithms for assembling the dual mesh. *Applied Numerical Mathematics*, 56 (6):778–799, JUN 2006. ISSN 0168-9274. doi: 10.1016/j.apnum.2005.06.008.

C. Parés. Numerical methods for nonconservative hyperbolic systems: a theoretical framework. *SIAM Journal on Numerical Analysis*, 44:300–321, 2006.

C. Parés and M. Castro. On the well-balanced property of roes method for nonconservative hyperbolic systems.applications to shallow water systems. *ESAIM: M2AN*, 38(5):300–321, 2004.

L Pareschi, G Puppo, and G Russo. Central Runge-Kutta schemes for conservation laws. *SIAM Journal on Scientific Computing*, 26(3):979–999, 2005. ISSN 1064-8275. doi: 10.1137/S1064827503420696.

G. Parker. Surface-based bedload transport relation for gravel rivers. *J. Hydraul. Res.*, 28(4):417–436, 1990.

B.C. Phillips and A.J. Sutherland. Spatial lag effects in bed load sediment transport. *J. Hydraul. Res.*, 27(1):115–33., 1989.

A. Preissmann. Propagation des intumescences dans les canaux et rivires. *1er Congrs de lAssociation Franaise de Calcul, Grenoble, France*, pages 433–442, 1961.

JX Qiu and CW Shu. On the construction, comparison, and local characteristic decomposition for high-order central WENO schemes. *Journal of Computational Physics*, 183(1):187–209, NOV 20 2002. ISSN 0021-9991. doi: 10.1006/jcph.2002.7191.

S. Saiedi. Coupled modeling of alluvial flows. *J. Hydraul. Eng.*, 123(5):440–446, 1997.

S.B. Savage and K. Hutter. The dynamics of avalanches of granular materials from initiation to run-out. *Acta Mech.*, 86:201–223, 1991.

C.W. Shu. Essentially non-oscillatory and weighted essentially non-oscillatory schemes for hyperbolic conservation laws. *Technical Report 97-65, NASA, Langley Research Center, Hampton,Virginia, USA,*, pages 202–228, 1997.

J. Sieben. *Modelling of hydraulics and morphology in mountain rivers.* PhD thesis, Delft University, 1997. also 'Communications on hydraulic and geotechnical engineering. Rep. No. 97(3), Delft Univ. of Technology, Delft, The Netherlands.

J Sieben. A theoretical analysis of discontinuous flow with mobile bed. *Journal of Hydraulic Research*, 37(2):199–212, 1999. ISSN 0022-1686.

E. F. Toro. On Glimm–Related Schemes for Conservation Laws. Technical Report MMU–9602, Department of Mathematics and Physics, Manchester Metropolitan University, UK, 1996.

E. F. Toro and S. J. Billett. Centred TVD Schemes for Hyperbolic Conservation Laws. *IMA J. Numerical Analysis*, 20:47–79, 2000.

E.F. Toro. Primitive, conservative and adaptive schemes for hyperbolic conservation laws. In *Numerical Methods for Wave Propagation.*, pages 323–385, 1998.

E.F. Toro. Anomalies of conservative methods: analysis, numerical evidence and possible cures. . *Computational Fluid Dynamics Journal*, 11(2):128–143, 2002.

E.F. Toro. *Riemann Solvers and Numerical Methods for Fluid Dynamics (2nd edn).* Springer: Berlin, 1999.

E.F. Toro. *Shock capturing methods for free-surface shallow flows.* John Wiley and Sons, LDD., 2001.

E.F. Toro and A. Siviglia. PRICE: Primitive centred schemes for hyperbolic system of equations. *International Journal for Numerical Methods in Fluids*, 42:1263–1291, 2003.

E.F. Toro and VA Titarev. Solution of the generalized Riemann problem for advection-reaction equations. *Proceedings Of The Royal Society Of London Series A-Mathematical Physical And Engineering Sciences*, 458(2018):271–281, 2002. ISSN 1364-5021.

E.F.. Toro, A. Hidalgo, and M. Dumbser. Force schemes on unstructured meshes i: conservative hyperbolic systems. *Journal of Computational Physics*, In press, 2009.

I Toumi. A weak formulation of Roe's approximate riemann solver. *Journal Of Computational Physics*, 102(2):360–373, OCT 1992. ISSN 0021-9991.

ME Vazquez-Cendon. Improved treatment of source terms in upwind schemes for the shallow water equations in channels with irregular geometry. *Journal Of Computational Physics*, 148(2):497–526, JAN 20 1999. ISSN 0021-9991.

A.I. Volpert. The space BV and quasilinear equations. . *Math. USSR Sbornik*, 73(2):225–267, 1967.

S Vukovic and L Sopta. ENO and WENO schemes with the exact conservation property for one-dimensional shallow water equations. *Journal Of Computational Physics*, 179(2):593–621, JUL 1 2002. ISSN 0021-9991. doi: 10.1006/jcph.2002.7076.

W. Wu, D. Vieira, and S. Wang. Onedimensional numerical model for nonuniform sediment transport under unsteady flows in channel networks. *Journal of Hydraulic Engineering, ASCE*, 130(9):914–923, 2004.

YL Xing and CW Shu. High order well-balanced finite volume WENO schemes and discontinuous Galerkin methods for a class of hyperbolic systems with source terms. *Journal Of Computational Physics*, 214(2):567–598, MAY 20 2006. ISSN 0021-9991. doi: 10.1016/j.jcp.2005.10.005.

M. Zennaro. Natural continuous extension of runge-kutta methods, mathematics

of computation 46. *Journal of Hydraulic Engineering, ASCE*, 46:119–133., 1986.

JG Zhou, DM Causon, CG Mingham, and DM Ingram. The surface gradient method for the treatment of source terms in the shallow-water equations. *Journal Of Computational Physics*, 168(1):1–25, MAR 20 2001. ISSN 0021-9991.

JG Zhou, DM Causon, DM Ingram, and CG Mingham. Numerical solutions of the shallow water equations with discontinuous bed topography. *International Journal for Numerical Methods in Fluids*, 38(8):769–788, MAR 20 2002. ISSN 0271-2091. doi: 10.1002/fld.243.